NUREG/CR-0202
ANL-78-53

NUREG/CR-0202
ANL-78-53

GRASS-SST: A Comprehensive, Mechanistic Model for the Prediction of Fission-gas Behavior in UO_2-base Fuels during Steady-state and Transient Conditions

by

J. Rest

ARGONNE NATIONAL LABORATORY, ARGONNE, ILLINOIS

Prepared for the U. S. NUCLEAR REGULATORY COMMISSION
under Interagency Agreement DOE 40-550-75

Available from
National Technical Information Service
Springfield, Virginia 22161

NUREG/CR-0202
ANL-78-53

Distribution Code: R-3

ARGONNE NATIONAL LABORATORY
9700 South Cass Avenue
Argonne, Illinois 60439

GRASS-SST: A Comprehensive, Mechanistic Model for the Prediction of Fission-gas Behavior in UO_2-base Fuels during Steady-state and Transient Conditions

by

J. Rest

Materials Science Division

Published: June 1978

Prepared for the Division of Reactor Safety Research
U. S. Nuclear Regulatory Commission
Washington, D. C. 20555
Under Interagency Agreement DOE 40-550-75

NRC FIN No. A2016

TABLE OF CONTENTS

TABLE OF CONTENTS

LIST OF FIGURES

LIST OF FIGURES

LIST OF TABLES

GRASS-SST: A Comprehensive, Mechanistic Model for the Prediction of Fission-gas Behavior in UO_2-base Fuels during Steady-state and Transient Conditions

by

J. Rest

ABSTRACT

The steady-state and transient gas release and swelling subroutine (GRASS-SST) is a mechanistic computer code for predicting fission-gas behavior in UO_2-base fuels. GRASS-SST treats fission-gas release and fuel swelling on an equal basis and simultaneously treats all major mechanisms that influence fission-gas behavior. The GRASS-SST transient analysis has evolved through comparisons of code predictions with the fission-gas release and physical phenomena that occur during reactor operation and transient direct-electrical-heating (DEH) testing of irradiated light-water reactor fuel. The GRASS-SST steady-state analysis has undergone verification for end-of-life fission-gas release and intragranular bubble-size distributions. The results of GRASS-SST predictions for transient fission-gas release during DEH tests are in good agreement with experimental data. Comparisons of GRASS-SST predictions of gas release and bubble-size distributions with the results of DEH transient tests indicate that (1) coalescing bubbles do not have sufficient time to grow to equilibrium size during most transient conditions, (2) mobilities of fission-gas bubbles in UO_2 are enhanced during nonequilibrium conditions if the excess pressure in the bubble is sufficient to generate an equivalent stress greater or equal to the yield stress of the surrounding matrix, and (3) channel formation on grain surfaces and coalescence of the channels with each other and with the tunnels of gas along the grain edges can contribute to grain-boundary separation and/or the rapid, long-range interconnection of porosity. The phenomena of grain-boundary separation and/or long-range interconnection of porosity provides an important release mechanism for fission gas that has moved out of the grains of irradiated fuel.

I. INTRODUCTION

The Steady-State and Transient Gas Release and Swelling Subroutine (GRASS-SST) is based on the GRASS code first reported by Poeppel.[1] GRASS was originally developed for the prediction of fission-gas behavior in Liquid Metal Fast Breeder Reactor (LMFBR) fuel during steady-power irradiations and was designed to be compatible with the LIFE LMFBR fuel-performance code.[2,3] Whereas GRASS was primarily concerned with intragranular fission-gas phenomena, GRASS-SST includes models for intra- and intergranular fission-gas-bubble behavior as well as a mechanistic description of the role of grain-edge interlinked porosity on fission-gas release and swelling. In general, GRASS-SST has evolved through comparisons of code predictions with the fission-gas releases and physical phenomena that occur during Light Water Reactor (LWR) operation, and during transient Direct Electrical Heating (DEH) tests on irradiated LMFBR and LWR fuel.[4-10] The DEH tests are specifically designed to aid in developing and verifying the GRASS-SST transient analysis.

The influence of fission gases produced in oxide fuels during irradiation on fuel performance has been the subject of many investigations over the past 20 years.[11] The inert fission gases are known to precipitate into bubbles. The bubbles grow as a result of bubble motion and coalescence and diffusion of gas atoms to bubbles. The growing bubbles cause the fuel to swell. In addition, fission-gas bubbles retained in the fuel on grain surfaces and edges can cause radical changes in the fuel microstructure. These changes in the fuel microstructure can then result in an enhanced gas release and/or fuel swelling.[5,7]

Fission-gas released from the fuel to the fuel-rod plenum and fuel-cladding gap stresses the cladding, degrades the thermal conductivity of the gap-gas mixture, and thus increases the fuel-rod operating temperatures. Fission-gas behavior during normal operation is fairly well known and is considered in fuel design. The effects of fission-gas on the behavior of the fuel are not well known and may be more severe during off-normal conditions than for steady-power irradiations because of increased fuel temperatures. Large stresses on the cladding can lead to cladding rupture, whereas excessive fuel temperatures can result in fuel melting.

In general, models developed over the past 20 years to predict the behavior of fission gases in oxide fuels have enjoyed limited success. They have evolved through the synergistic interplay of mechanisms for fission-gas behavior. As limitations in the predictive capability of the models were discovered, additional mechanisms thought to have a dominant effect on fission-gas release and swelling were included. For example, the early Booth model[12] was based on the diffusion of gas atoms in a concentration gradient within a spherical volume to the surface of the sphere where the gas was assumed to be released. Yuill et al.[13] enlarged on the Booth model by including the effects

of temperature gradients and by assuming that the gas atoms were released when the gas reached the pellet surface rather than being released from the boundary of an "equivalent" volume. MacEwan and Stevens[14] and Carroll et al.[15] included the effects of gas-atom trapping based on the results of experiments that indicated a decrease in diffusion coefficient with an increase in fission rate and exposure.

In the early 1960's, observations of fission-gas bubbles in irradiated UO_2 introduced the possibility that fission-gas release might be controlled by bubble behavior rather than by atomic diffusion.[16] In addition, it was demonstrated that fission-gas bubbles could be destroyed as a result of re-solution of gas atoms from bubbles in a radiation field.[17] Subsequently, the substantial effect of grain-edge interlinked porosity on gas release and fuel swelling was demonstrated.[18,19] Finally, transient heating tests[5,7] on irradiated fuel have indicated that fission-gas-bubble behavior may have an important effect on the evolution of the fuel microstructure by causing grain-boundary separation. Grain-boundary separation can then provide pathways that permit the trapped fission gas to escape from the fuel.

Any model that attempts a realistic description of fission-gas release and swelling as a function of fuel-fabrication variables and a wide range of reactor operating conditions must treat fission-gas release and fuel swelling as coupled phenomena and must include many mechanisms influencing fission-gas behavior. In addition, a mechanistic treatment of fission-gas phenomena includes the potential for a predictive capability outside the range of conditions used for model verification.

GRASS-SST calculations include the effects of production of gas from fissioning uranium atoms, bubble nucleation, a realistic equation of state for xenon, lattice bubble diffusivities based on experimental observations, bubble diffusion, bubble migration, bubble coalescence, re-solution, temperature and temperature gradients, interlinked porosity, and fission-gas interaction with structural defects on both the distribution of fission-gas within the fuel and on the amount of fission-gas released from the fuel. GRASS-SST calculates the fission-gas-induced swelling due to, and the fission-gas-bubble-size distribution for, bubbles in the lattice, on grain boundaries, on dislocations, and along the grain edges, and the total fission-gas release as a function of time for steady-state and transient conditions. Fission gas released from the fuel reaches the fuel surface by successively diffusing from the grains to grain boundaries and then to the grain edges, where the gas is released through a network of interconnected tunnels of fission-gas and fabricated porosity.

Phenomena identified through comparisons of code predictions with DEH experimental results have been included in the GRASS-SST analysis.[8] In particular, GRASS-SST includes the effects of the degree of nonequilibrium in the UO_2 lattice on fission-gas bubble mobility and bubble coalescence. GRASS-SST also accounts for the observed formation of grain-surface channels[7]

which, in addition to providing a direct path through which gas residing on the grain surfaces can reach the grain edges, can coalesce with each other as well as with the grain-edge tunnels and therefore contribute to intergranular separation and/or cause long-range pore interlinkage. This concept of fission-gas release is in strong contrast to earlier models, many of which are based on the assumption that the gas is released once it encounters a grain boundary. Sections II and III describe the models included and the calculational procedure used in the GRASS-SST code, respectively, in detail. In Sec. IV, the numerical procedure used in GRASS-SST is benchmarked. Sections V and VI, respectively, describe verification results and sensitivity analyses obtained with the code for the behavior of fission gas in oxide fuels under steady-state conditions. Section VII presents models for phenomena identified through a comparison of code predictions with DEH experimental results and gives the results of the verification of the GRASS-SST transient analyses. Section VIII discusses the extension of phenomenology observed during transient heating to the description of high burnup gas release. Finally, in Sec. IX the conclusions of the present work are summarized.

II. DESCRIPTION OF BASIC MODELS

A. Intragranular Fission Gas

The rate of fission-gas production, η, is assumed to occur primarily within the UO_2 grains and is assumed proportional to the fission rate, β. That is,

$$\eta = \alpha\beta, \tag{1}$$

where α is the number of gas atoms produced per fission event. The noble gases xenon and krypton are very insoluble in the UO_2 lattice and tend to nucleate into fission-gas bubbles. The nucleation rate, N_R, at which gas atoms combine to form two atom clusters is given by

$$N_R = f_N C_{II}, \tag{2}$$

where C_{II} is the rate at which gas atoms collide, and f_N, the nucleation factor, is the probability that two atoms that have come together actually coalesce. Coalescence may require the proximity of one or more vacancies or vacancy clusters.[20]

The basic equations for intragranular bubble coalescence in GRASS-SST are the same as those used by Gruber,[21] but the calculational procedure is more approximate. In general, the determination of the fission-gas bubble-size distribution requires the simultaneous solution of an extremely large set of coupled nonlinear integral-differential equations for bubbles from a few angstroms (single gas atom) to many microns in radii. No exact analytical solution exists for this class of problem.

For the purpose of calculation (i.e., reasonable code running times), the bubbles are classified by an average size, where size is defined in terms of the number of gas atoms per bubble. This method of bubble grouping significantly reduces the number of equations needed to describe the bubble-size distributions. The bubble classes are ordered so that the first class refers to bubbles that contain only one gas atom. If S_i denotes the average number of atoms per bubble for bubbles in the ith class (called i bubbles henceforth), then the bubble-size classes are defined by

$$S_i = mS_{i-1}, \tag{3}$$

where the integer $m \geq 2$, $i \geq 2$, and $S_1 = 1$. The S_1 class is assumed to consist of a single gas atom associated with one or more vacancies or vacancy clusters. In the lattice, P_{ij}^R and P_{ij}^B, the probabilities in cm^3/s of an i bubble coalescing with a j bubble, where the bubbles move by random (motion in a concentration gradient) and biased (motion in a temperature gradient) migration, respectively, are given by[21]

$$P_{ij}^R = 4\pi(r_i + r_j)(D_i^\ell + D_j^\ell), \quad \text{random}, \tag{4}$$

and

$$P_{ij}^B = \pi(r_i + r_j)^2|v_j - v_i|, \quad \text{biased}, \tag{5}$$

where r_i is the average i-bubble radius (mm), D_i^ℓ is the average lattice i-bubble diffusion coefficient (mm^2/s), and v_i is the velocity (mm/s) of an i bubble moving in a temperature gradient.

Assume $i \geq j$ in all cases. The rate of coalescence C_{ij} of i bubbles with j bubbles is given by

$$C_{ij} = P_{ij}F_iF_j, \tag{6}$$

where

$$P_{ij} = P_{ij}^R + P_{ij}^B \tag{7}$$

and F_i is the number of i bubbles per unit volume. For $i = j$, C_{ij} becomes

$$C_{ii} = \tfrac{1}{2}P_{ii}F_i^2, \tag{8}$$

so that each pairwise coalescence is counted only once.

Coalescence between bubbles results in bubbles growing from one size class to another. The probability that a coalescence between an i bubble and a j bubble will result in a k bubble is given by the array T_{ijk}.[20] The number of gas atoms involved in one such coalescence is $S_i + S_j$. The array T_{ijk} is defined by the three conditions:

1. The total probability of producing a bubble is unity; i.e., $\sum_k T_{ijk} = 1$.

2. The number of gas atoms, on the average, is conserved; i.e., $\sum_k T_{ijk} S_k = S_i + S_j$.

3. For a given pair ij, only two of the T_{ijk} array elements (corresponding to k and k + 1, where $S_k \leq S_i + S_j \leq S_{k+1}$; i.e., $m \geq 2$) can be nonzero.

From these three conditions, it follows that $k = i$, and

$$T_{ijk} S_k + (1 - T_{ijk}) S_{k+1} = S_i + S_j. \tag{9}$$

Thus, the probability that a coalescence between an i bubble and a j bubble results in a k bubble is given by

$$T_{ijk} = \frac{S_{k+1} - S_i - S_j}{S_{k+1} - S_k} = 1 - \frac{S_j}{S_{k+1} - S_k}, \tag{10}$$

and the probability that the coalescence results in a k + 1 bubble is given by

$$T_{ijk+1} = \frac{S_i + S_j - S_k}{S_{k+1} - S_k} = \frac{S_j}{S_{k+1} - S_k}. \tag{11}$$

The array T_{ijk} may be considered as the probability that an i bubble becomes a k bubble as a result of its coalescence with a j bubble. The rate N_{ik} at which i bubbles become k bubbles is given by

$$N_{ik} = \sum_{j \leq i} C_{ij} T_{ijk}. \tag{12}$$

The j bubble is assumed to disappear; gas atoms are absorbed into the i bubble. The rate χ_j of disappearance is given by

$$\chi_j = \sum_{i \geq j} C_{ij}. \tag{13}$$

The rate N_{ik} at which i bubbles become k bubbles, with $k = i + 1$, is reduced by the re-solution of gas atoms. Re-solution is the result of a direct

(or possibly indirect) collision between a fission fragment and a gas bubble. From Eqs. 11 and 12,

$$N_{ik} = \sum_{j \leq i} C_{ij} T_{ijk}$$

$$= \sum_{j \leq i} P_{ij} F_i F_j \frac{S_j}{S_k - S_i}$$

$$= \frac{F_i}{S_k - S_i} \sum_{j \leq i} P_{ij} F_j S_j. \tag{14}$$

The expression

$$\sum_{j \leq i} P_{ij} F_j S_j$$

is the rate at which gas atoms are added to an i bubble. Re-solution causes an i bubble to lose gas atoms at a rate given by $b_i S_i$, where b_i is the probability that a gas atom in an i bubble is redissolved. The reduced N_{ik} becomes

$$N_{ik} = \frac{F_i}{S_k - S_i} \sum_{j \leq i} (P_{ij} F_j S_j - b_i S_i). \tag{15}$$

If the expression within parentheses is negative, then N_{ik} is zero, and $N_{ik'}$, the rate at which i bubbles become i - 1 bubbles with k' = i - 1, is defined as

$$N_{ik'} = \frac{F_i}{S_i - S_{k'}} (b_i S_i - \sum_{j \leq i} P_{ij} F_j S_j). \tag{16}$$

Equations 15 and 16 are proportional to the probabilities that any particular i bubble becomes an i + 1 or an i - 1 bubble, respectively; the ratio of the probabilities is equal to the ratio of the rates. Clearly, the above definitions N_{ik} and $N_{ik'}$ are consistent with the conservation of the total number of gas atoms.

The model for the i bubble re-solution constant is based on the work of Nelson[22] and is given by

$$b_i = \beta b_0 [1 - r_i/(r_i + r_d)], \tag{17}$$

where β is the fission rate (fissions/m^3·s), r_d is the average distance an ejected atom travels from the bubble surface, and b_0 is a constant. The re-solution rate decreases as the bubble size increases. This is due to a decreased probability of escape for an ejected atom. This model for single gas-atom re-solution from bubbles is in contrast to some theories which assume whole bubble destruction (for small bubbles) as a result of a single collision between a fission fragment and a fission-gas bubble.[23]

B. Fission Gas Pinned to Dislocations

The atomic fission gas diffuses by random migration to dislocations at a rate governed by[24]

$$R_1^d = \frac{2\pi D_1^{\ell} \rho c}{\ell n(r_c/r_1)}, \tag{18}$$

where ρ is the dislocation density (mm/mm^3), c is the concentration of fission gas in the lattice, r_1 is the mathematical radius of a single gas atom, and r_c is the radius of the cylindrical capture volume; i.e.,

$$(\pi r_c^2)\rho = 1. \tag{19}$$

The fission gas can also migrate to dislocations in a temperature gradient. In this case, the rate of migration of an i bubble is given by

$$B_i^d = 2\rho r_i v_i. \tag{19}$$

Once the fission gas is pinned to dislocations, the gas can coalesce with both lattice and dislocation bubbles (re-solution causes gas atoms to be knocked back into the lattice), and the gas can be pulled back into the lattice by the force of a temperature gradient if the fission-gas bubbles grow beyond a specified critical size.[25] Coalescence probabilities for bubbles on dislocations can be derived based on a solution of the one-dimensional, time-independent diffusion equation and are given by

$$P_{ij}^R = \left(D_i^d + D_j^d\right)\Big/\sqrt{\rho} \tag{20}$$

and

$$P_{ij}^B = (v_i - v_j)/\rho, \tag{21}$$

where D_i^d is the average dislocation i-bubble diffusion coefficient. The coalescence probabilities for dislocation bubbles coalescing with lattice bubbles are given by Eqs. 4 and 5 with the diffusivity of the dislocation bubble equal to zero; i.e., the bubble on the dislocation is assumed pinned and immobile.

C. Intergranular Fission Gas

The fission gas migrates as gas atoms and in the form of gas bubbles from the UO_2 lattice (where the gas is generated) to grain boundaries by diffusion and also by biased migration in a temperature gradient. The diffusion of the atomic fission gas is a complex process in which the gas becomes

trapped by diffusion to fission-gas bubbles and is subsequently released by re-solution after an average wait period. The GRASS-SST model for fission-gas diffusion to the grain boundaries is a generalization of a calculation by Speight.[26] Speight solved the problem of fission-gas atom diffusion from the lattice to the grain boundaries by assuming that the deposition of gas, produced at a rate η per unit volume per second, satisfied the equations

$$\left.\begin{aligned} \frac{\partial c}{\partial t} &= \eta + D_I^{\ell}\nabla^2 c - gc + bu \\ \text{and} \\ \frac{\partial u}{\partial t} &= gc - bu \end{aligned}\right\}, \tag{22}$$

where $c = c(r,t)$ is the local average concentration of gas in solution, u is the corresponding amount of gas per unit volume in bubbles, D_I^{ℓ} is the atomic diffusivity of fission gas in the lattice, g is the probability per second of a gas atom in solution being captured by a bubble, and b is the corresponding probability per second of a gas atom within a bubble being redissolved.

Speight solved Eq. 22 subject to the boundary conditions

$$\left.\begin{aligned} c(a,t) &= 0 \\ \text{and} \\ c(r,0) &= 0 \end{aligned}\right\}, \tag{23}$$

where a is the grain radius. However, the boundary conditions listed in Eq. 23 are not suitable for certain classes of important problems. For example, Eqs. 22 and 23 are not applicable under load-following conditions when the fission rate, β, changes as a function of time. In addition, the GRASS-SST code is used to simulate a steady-state reactor irradiation ($\beta \neq 0$, $b \neq 0$, $g \neq 0$) followed by an out-of-reactor DEH heating ramp ($\beta = b = 0$, $g \neq 0$). The boundary conditions for Eqs. 22 applicable under these conditions are

$$\left.\begin{aligned} c(a,t) &= C_g(t) \\ \text{and} \\ c(r,t_0) &= C_I(t_0). \end{aligned}\right\}. \tag{24}$$

In keeping with the spirit of the GRASS-SST calculational procedure, the calculation of intragranular gas-atom diffusion to grain surfaces is treated as follows. The solution to Eqs. 22 subject to the boundary conditions listed in Eq. 24 can be shown to be equivalent to the sum of the solutions of two separate problems: the solution of Eqs. 22 and 23, and the solution of

$$\left.\begin{aligned} \frac{\partial c}{\partial t} &= D_I^{\ell}\nabla^2 c - gc + bu \\ \text{and} \\ \frac{\partial u}{\partial t} &= gc - bu \end{aligned}\right\}, \tag{25}$$

with the boundary conditions listed in Eq. 24.

Equations 22 and 23 will be valid for constant $\dot{\eta}$ from $t = 0$ to $t = t_0$; at $t = t_0$, $\dot{\eta}$ changes to $\dot{\eta}'$, and from $t = t_0$ to $t = t_1$, the solution is the sum of the solutions of Eqs. 22 and 23 and Eqs. 24 and 25 with t replaced by t', where $t' = t - t_0$, and $C_I(t_0)$ is the intragranular gas concentration at $t = t_0$. Between $t = t_1$ and $t = t_2$, when the gas production rate is $\dot{\eta}''$, the solution is obtained in an analogous fashion. The approximation, $c(a,t) = 0$ for the first time interval is quite good, since the fission-gas concentration on the grain boundaries early in life is very small. Under transient DEH test conditions, the solution for intragranular fission-gas diffusion is obtained from Eqs. 24 and 25 with t replaced by h, the code time increment; $C_I(t)$ and $C_g(t)$ are computed as a function of time.

For irradiation times t such that

$$(b + g)a^2/D_I^{\ell}\pi^2 > bt > 5, \tag{26}$$

Speight[26] derived an approximate solution to Eqs. 22 and 23 for the fractional fission-gas release f_{gr}, given by

$$f_{gr} = \frac{4}{a}\left[\frac{D_I^{\ell} bt}{\pi(b + g)}\right]^{1/2} - \frac{3D_I^{\ell} bt}{2a^2(b + g)}. \tag{27}$$

This expression is analogous to that derived by Booth[12] for gas-atom diffusion (with no trapping) if an effective diffusion coefficient is defined by

$$D_{eff}^{\ell} = D_I^{\ell}\frac{b}{b + g} \tag{28}$$

The factor $b/(b + g)$ is the probability that, at a given time, a particular gas atom is dissolved, and hence becomes a freely mobile species. For the rest of the time, the gas atom is bound within relatively stationary bubbles.

The GRASS-SST calculation uses the rate of intragranular gas-atom diffusion to grain boundaries. The rate of fission-gas-atom diffusion to the grain boundaries, R_I^g, can be obtained from Eq. 27 from

$$R_i^g = \eta \frac{d(f_{gr}t)}{dt}, \tag{29}$$

where R_i^g is in atoms/mm^3·s. Thus,

$$R_i^g = \frac{6\eta}{a}\left[\frac{D_i^\ell bt}{\pi(b+g)}\right]^{1/2} - \frac{3D_i^\ell bt\eta}{a^2(b+g)}. \tag{30}$$

In an analogous fashion to the derivation of Eq. 30, an approximate expression for the rate of fission-gas diffusion to grain boundaries can be obtained from a solution to Eqs. 24 and 25. The result is

$$R_i^g = 3(C_I - C_g)\left\{\left[\frac{D_i^\ell b}{a^2(b+g)(t-t_0)}\right]^{1/2} - \frac{D_i^\ell b}{a^2(b+g)}\right\}. \tag{31}$$

The sum of Eqs. 30 and 31 represents an approximate solution of Eqs. 22 and 24 for the rate of intragranular gas-atom diffusion to grain boundaries, valid for the range of irradiation times specified by Eq. 26.

During a DEH transient-heating ramp, $\beta = b = 0$. An approximate solution for these conditions can be obtained by setting $b/(b+g) = 1$ in Eq. 31. The approximation is quite good in light of the solution procedure outlined above; that is, $C_I(t)$ and $C_g(t)$ are recomputed for every time increment and indirectly contain the effect of the trapping of gas atoms by bubbles. This solution will be valid for GRASS-SST time increments, h, that satisfy the condition[12]

$$\frac{\pi^2 D_i^\ell h}{a^2} \leq 1. \tag{32}$$

Fission-gas bubbles can migrate to the grain boundaries in a temperature gradient. (The migration of bubbles to the grain boundaries by Brownian motion was determined to be small.) The rate of bubble migration is given by

$$B_i^g = S_v^{\alpha\alpha}, \tag{33}$$

where $S_v^{\alpha\alpha}$ is the grain-boundary area per unit volume. (This expression is very approximate for small bubbles.)

Once on the grain boundaries, the fissior gas can coalesce (re-solution is operative; a fraction of all ejected atoms are assumed to be knocked back into the lattice), the gas can be pulled back into the lattice by the force of a temperature gradient if the fission-gas bubbles reach a certain critical size,[25] and the gas can migrate to the grain edges. Coalescence probabilities for bubbles on grain boundaries can be derived based on a solution of the time independent two-dimensional diffusion equation and are given by

$$P_{ij}^{R} = (D_i^g + D_j^g)/S_v^{\alpha\alpha} \tag{34}$$

and

$$P_{ij}^{B} = 2(v_i - v_j)(r_i + r_j)/S_v^{\alpha\alpha} \tag{35}$$

where D_i^g is the average grain-boundary-bubble diffusion coefficient.

D. Rate of Growth of Coalescing Bubbles during Transient Conditions

During steady-state conditions, it is reasonable to assume that, when two fission-gas bubbles coalesce, the noninstantaneous rate of growth of the resultant bubble to equilibrium size can be treated as instantaneous.[27] However, in a transient analysis, this assumption breaks down, and the noninstantaneous rate of growth of coalescing bubbles must be included. The need for a GRASS-SST model that describes the limited rate of growth of coalescing bubbles became apparent when GRASS-SST-calculated bubble-size distributions for DEH test conditions were compared with qualitative experimental observations. The code predicted similar end-of-test bubble distributions in the lattice and on the grain boundaries. However, the observed intragranular bubble densities were much lower than predicted. A similar conclusion concerning the need to include the effects of nonequilibrium coalescing bubbles in the analysis of fission-gas behavior during transient conditions was reported in a comparison of fission-gas release and swelling (FRAS) code predictions with DEH tests on irradiated mixed-oxide fuel.[28]

In general, when two bubbles initiate coalescence, a strain field is generated in the lattice around the growing bubble. Initially, bubble coalescence is a volume-conserving process. Subsequently, vacancies that move under the influence of the strain field migrate to the bubble, resulting in an increase in the bubble volume. As vacancies enter the growing bubble, the strain field gradually relaxes and vanishes (to first order) when the bubble has reached its equilibrium size.

A bubble-relaxation time, τ_i, can be defined such that, at a time $t = t_i$ after the initiation of bubble coalescence, the resultant bubble has approached a stable configuration by an amount $1 - 1/e$. A precise determination of τ_i is not within the scope of the GRASS-SST calculations at this time. However, τ_i can be estimated from a consideration of lattice-vacancy thermodynamics. The rate equations for the bubble radii and the lattice vacancy concentration will be described to illustrate the approximations involved in estimating τ_i. Let r_i be the sum of the radii of the coalescing bubbles. If primary creep is neglected, the rate of growth of r_i is given by[27,29]

$$\frac{dr_i}{dt} = \frac{D_v}{r_i}\left[c_v - c_v^e \exp(-P_i^{ex}\Omega/kT\right]. \tag{36}$$

In Eq. 36, c_v^e is the fractional equilibrium vacancy concentration given by

$$c_v^e = \exp(-E_v^f/kT), \tag{37}$$

D_v is the vacancy diffusion coefficient given by

$$D_v = D_v^0 \exp(-E_v^m/kT), \tag{38}$$

E_v^f and E_v^m are the vacancy formation and migration energies, respectively, D_v^0 is a preexponential factor, Ω is the atomic volume, P_i^{ex} is the excess internal gas pressure for each bubble of radius r_i given by

$$P_i^{ex} = P_i^g(T) - \frac{2\gamma}{r_i}, \tag{39}$$

where γ is the effective surface tension, and P_i^g is the gas pressure within a bubble of radius r_i at temperature T. The explicit rate equation for $c_v(T)$ is given by[29]

$$\frac{dc_v}{dt} = -4\pi D_v c_v \sum_{i=1}^{N} r_i C_i + 4\pi D_v c_v^e \sum_{i=1}^{N} r_i C_i \exp(-P_i^{ex}\Omega/kT)$$

$$+ \frac{12\sqrt{\pi}}{d} D_v \left(\sum_{i=1}^{N} r_i C_i \right)^{1/2} (c_v^e - c_v), \tag{40}$$

where C_i is the concentration of bubbles of radius r_i, and d is the grain diameter.

To determine the variation of P_i^{ex} requires solving the simultaneous rate Eqs. 36 and 40 for $r_i(t)$ and $c_v(t)$. Obviously, Eqs. 36 and 40 can only be solved numerically. However, the dimensional form of the two contributions to $\dot{c}_v$ and the term in $\dot{r}_i$ suggests three relaxation times:[29] one for the vacancy concentration where the vacancies are supplied by bubbles, one for the vacancy concentration where the vacancies are supplied by grain boundaries, and one for the growth of bubbles given by

$$\tau_i^B = \frac{r_i^2}{D_v c_v^e}. \tag{41}$$

In the following discussion, we shall assume that the rate of growth of non-equilibrium bubbles can be qualitatively characterized by Eq. 41.

Instead of directly calculating the individual fission-gas bubble behavior, GRASS-SST groups the continuum of bubble sizes into a relatively small number of bubble-size classes with each size class, i, characterized by an average bubble radius, r_i. The basic GRASS-SST calculation is for the rate at which bubbles grow from the i to the i + 1 size class. The motivation for treating the problem from this level is that much less computer time is required. The effect of a limited rate of growth of coalescing bubbles on the GRASS-SST calculation is a reduction in the rate at which bubbles grow from the i into the i + 1 size class by the amount

$$[1 - (1 - \varkappa)\exp(-\Delta t/\tau_i^B)], \tag{42}$$

where Δt is the code time step (i.e., the fuel temperatures and stresses are assumed constant during Δt), and $\varkappa$ ($0 \leq \varkappa \leq 1$) corresponds to the bubble-class transfer rate that would exist in the total absence of point-defect motion. Eq. 42 is used for both intra- and intergranular fission-gas-bubble coalescence. However, one would expect that, because of enhanced grain-boundary-vacancy diffusion, the grain-boundary-bubble relaxation times would, in general, be smaller than the lattice-bubble relaxation times.

E. Gas-channel Formation on Grain Boundaries

The SEM examinations of DEH-tested fuel, described in Ref. 5, revealed the development of sinuous channels on the grain faces after a saturation density of grain-boundary fission gas has been attained. These face channels link up and extend to the grain-edge channels, thus enhancing the release of the gas from the grain surfaces.

The GRASS-SST model for grain-boundary saturation by fission-gas bubbles is based on the fact that the grain-boundary area occupied by fission-gas bubbles is nearly independent of the bubble-size distribution. (That is, the bubble-surface area is conserved after bubble coalescence.) If the gas is assumed to occupy equal, close-packed, touching bubbles, then the maximum areal coverage per unit area of grain boundary is $A^* = 0.907$. Since the bubble size does not affect the atom areal density, the areal coverage by the fission gas is approximately equal to the coverage by a single bubble of radius r_{max}, formed by the coalescence of all the gas on the grain face. The assumption that the bubble-surface area is conserved after bubble coalescence leads directly to an expression for r_{max} in terms of the total number of bubbles on the boundary; i.e.,

$$r_{max} = r_i\sqrt{N_i}, \tag{43}$$

where all bubbles on the grain face are assumed to have radius r_i, and N_i is the total number of bubbles. The condition for grain-boundary saturation by fission gas is then given by

$$\pi r_{max}^2 = \frac{4}{3}\pi a^3 A^* \frac{S_v^{\alpha\alpha}}{14}, \tag{44}$$

where an approximate tetrakaidecahedral (14-sided) lattice geometry has been assumed. In Eq. 44, a is the grain radius and $S_v^{\alpha\alpha}$ is the grain-boundary area per unit volume. Combining Eqs. 43 and 44 leads to an expression for $N_A^{sat}(i)$, the minimum number of gas bubbles with radius r_i per unit area of grain boundary required for saturation:

$$N_A^{sat}(i) = \frac{0.395A^*}{14\pi r_i^2} = \frac{0.008}{r_i^2}, \tag{45}$$

where $S_v^{\alpha\alpha} = 1.185/a$. For example, the minimum number of 500-Å-dia (5×10^{-5}-mm-dia) bubbles per unit area of grain boundary required for saturation is

$$N_A^{sat}(500) = \frac{0.008}{r_{500}^2} = 1.3 \times 10^7 \text{ bubbles/mm}^2. \tag{46}$$

This result is in reasonable agreement with the measured 500-Å (5×10^{-5}-mm) grain-boundary bubble-saturation density of $2.2\text{-}4.2 \times 10^7/\text{mm}^2$ (Ref. 30).

F. Fission Gas along Grain Edges

The GRASS-SST calculation for the diffusion of fission-gas atoms from the grain boundaries to the grain edges is based on a model by Fisher[31] for diffusion in an isotropic slab. Fisher assumed that the grain boundary could be represented as a uniform isotropic slab of material of width δ within which diffusion occurs according to Fick's laws. Furthermore, he assumed that the matrix is infinite and an initially zero concentration of the diffusing material exists in the body. The diffusivity, D_l^g, in the boundary is assumed to be higher than the diffusion coefficient, D_l^ℓ, in the grain lattice on either side. Diffusion then proceeds along the slab (in the y direction).

Fisher calculated fission-gas-atom diffusion on grain boundaries by solving Fick's equations for gas on the boundary and within the grains subject to the boundary conditions of (a) continuity of composition at the transition between boundary and grains and (b) a boundary concentration at the surface, C_g, given by

$$c = C_g \text{ at } t \geq 0 \text{ and } y = 0. \tag{47}$$

The concentration distribution c(x, y, t) in a specimen that has a boundary perpendicular to the surface is then given approximately by

$$c(x, y, t) = C_g \exp(-\pi^{1/4}\varphi\alpha^{-1/2})\operatorname{erfc}(\xi/2), \tag{48}$$

where the dimensionless coordinates φ, ξ, and α are defined by

$$\varphi = \frac{y}{(D_1^g t)^{1/2}}, \quad \xi = \frac{x - \delta/2}{(D_1^g t)^{1/2}}, \quad \text{and} \quad \alpha = \frac{D_1^\ell}{D_1^g} \frac{\delta/2}{(D_1^g t)^{1/2}}. \tag{48a}$$

The average concentration, $\bar{c}$, in a plane y = constant is

$$\bar{c} = C_g \exp(-\pi^{1/4} \varphi \alpha^{-1/2}). \tag{49}$$

Integration over the entire length of the slab of the expression for $\bar{c}$ gives the total quantity of gas on the boundary after a time t, and differentiating this expression with respect to time gives the rate at which the gas is diffusing to the grain edges. In GRASS-SST, C_g is obtained as a function of time from the solution of the bubble-size distributions. Under these conditions, the time t is replaced by the code time increment h, and the rate of gas-atom diffusion to the edges is given by

$$R_1^e = \frac{C_g}{4hr_b} \{[1 - \exp(-\chi r_b)]/\chi - r_b \exp(-\chi r_b)\}, \tag{50}$$

where r_b is the effective distance the gas must travel before encountering an edge and χ is given by

$$\chi = \left(\frac{2D_1^\ell}{\delta D_1^g}\right)^{1/2} \left(\frac{\pi}{D_1^\ell h}\right)^{1/4}. \tag{51}$$

To determine r_b requires an assumption about the microstructure of the fuel. If the fuel is assumed to consist of an assembly of identical tetrakaidecahedral grains, then r_b can be approximated by

$$r_b = a/\sqrt{14}. \tag{52}$$

The fission gas can also migrate to the edges in a temperature gradient at a rate given by

$$B_i^e = v_i \cos \bar{\theta}/r_b, \tag{53}$$

where $\bar{\theta}$ is the average angle between the orientation of a grain boundary and the temperature gradient.

Fission gas that has migrated from the UO_2 grain surfaces to the grain edges remains trapped at the edges unless a path exists through which the gas can escape from the fuel. Tunnels of porosity along the grain edges have been

observed in irradiated fuel under a variety of conditions.[18] For fuel swelling below ~7%, the degree of interlinked porosity appears to be strongly dependent on the fuel microstructure (i.e., grain size, fuel density, and pore-size distribution). Above ~7% fuel swelling, extensive interlinkage of the edge porosity has been observed that results in a nearly complete network of open paths through which fission gas reaching the grain edges can escape.

In the GRASS-SST treatment of interlinked porosity, which is statistical in nature, the degree of pore interlinkage along the grain edges is a function of both the grain and pore-size distributions. The model, which is based on the mathematical theory of percolation,[32] uses the concept of an arbitrary distribution of sites with randomly distributed bonds or links that join pairs of sites. The concentration of bonds is given by

$$P = \frac{\text{number of bonds}}{\text{number of sites}}.$$

The model predicts[32] that long-range interlinkage of sites will occur for

$$P \geq 1.569. \tag{54}$$

As applied to nuclear fuel, the sites are represented by intergranular pores; a bond is formed when two adjacent pores become connected. In this case, the concentration of bonds, P, can be expressed as[33]

$$P = \tfrac{1}{2}CN\left[1 + (f_p^{-1} - 1)\frac{2CN}{\pi}\,\frac{1 - \sqrt{1 - \left(\frac{q}{1+q}\right)^2}}{q}\right]^{-1}, \tag{55}$$

which enables P to be calculated from the two experimental parameters f_p (the fractional porosity) and q (the ratio of grain size to pore size) and the geometrical factor CN (the coordination number for a compact arrangement of pores).

A first assumption for pore interlinkage would be to consider the condition $P > 1.57$ as the abrupt limit for intergranular release through percolation. Actually, P is a function of the local values and spatial variances of fractional porosity, pore size, and grain size. Therefore, a statistical distribution around an average value of P must be assumed. In this case, one obtains

$$\text{pore interlinkage fraction} = \frac{1}{\sigma\sqrt{2\pi}} \int_{x=1.57}^{\infty} \exp[-(x - P)^2/2\sigma^2]dx, \tag{56}$$

where σ (width of distribution of P) can be calculated from the experimental histograms of pore size, grain size, and fractional porosity.[33] The gas released

from a section of fuel is determined by the amount of gas reaching the pores multiplied by the pore interlinkage fraction; the remaining gas contributes to grain-edge swelling.

In contrast to the experimental results described in Refs. 5 and 18, the above formalism for calculating the evolution of interconnected porosity does not predict that a rapid increase in long-range porosity interconnection will occur after a critical value of swelling due to fission-gas bubbles has been reached. The reasons for this deficiency are (a) the geometry assumed in the above model does not correspond to observations of DEH- and PBF-tested fuel, (b) GRASS-SST does not include a realistic calculation of the pore-size distribution (pores in which the internal gas pressure is less than the surface-tension-induced pressure), and (c) material properties used in the GRASS-SST calculation of the pore-size distribution are experimentally almost inaccessible.

Thus, to provide a more realistic calculation of the pore-interlinkage fraction, the above model is supplemented by the additional criterion

$$\text{pore-interlinkage fraction} = 1.0, \quad \text{if } B_V > B_{Vcrit}, \tag{57}$$

where B_V is the calculated volume strain due to fission-gas bubbles, and B_{Vcrit} (0.07) is the critical gas-bubble volume fraction above which extensive long-range interconnection of the grain-edge tunnels is assumed to take place. If, subsequently, B_V becomes less than B_{Vcrit}, the edge tunnels are assumed to sinter shut, and the calculation of pore interlinkage is again performed via percolation theory. Turnbull and Tucker[18] observed that, in nontransient-tested UO_2, interlinked grain-edge tunnels were stable when the volume fraction was >0.07. The critical value for tunnel interlinkage in GRASS-SST is taken from their work.

Intergranular crack propagation has the potential to release fission gas that would otherwise be trapped on grain surfaces and edges. DEH transient heating tests indicate the likelihood of gas release by this mechanism.[5,7] However, the magnitude of the effect is unknown.

At the present stage of development, GRASS-SST does not contain models for the formation and interlinkage of the planar intergranular separations observed in DEH-tested fuel.[5,7,8] In particular, the contribution of these separations to the total swelling does not appear in the calculated value of B_V. As a result, B_{Vcrit} is smaller than the critical volume fraction (~0.18) measured in DEH transient experiments.[5,7]

G. Fission-gas-bubble Diffusivities during Steady-state Conditions

Estimates of the diffusivity of atomic xenon at 1500°C, based on the results of various experiments,[34] differ by as much as three orders of magnitude. Little is known about the bubble diffusivities in UO_2 at high temperatures

(>1500°C). For example, between 1800 and 2800°C (UO_2 melts at about 2850°C), there are six to seven orders of magnitude separating bubble diffusivities, based on an extrapolation of Gulden's measurements at 1500°C[35] and those obtained from the theory of surface diffusion.[21] In general, intragranular bubble transport by surface diffusion under typical steady-state conditions is thought unlikely.

Bubble movement by surface diffusion requires that the matrix atoms move out of the UO_2 crystal and onto the bubble surface easily, and vice versa. However, during equilibrium conditions, the bubbles may be faceted and thus will move slower through the solid than predicted by surface diffusion. The rate of motion of a faceted bubble has been shown to be determined by the frequency of nucleation of steps, instead of the time required for atoms to move from a step on one side of the bubble to a step on the other side.[36-39]

During steady-state conditions, GRASS-SST intragranular bubble diffusivities are assumed to have the form

$$D_i^{\ell} = D_1^{\ell}(r_1/r_i)^{1.62}, \tag{58}$$

where D_i^{ℓ} is the diffusivity of a bubble with radius r_i. For intragranular diffusion, the exponent in Eq. 58 was found[20] to have the value of 1.62 by fitting Eq. 58 to published experimental data. Above ~1250°C, the atomic diffusivity is assumed thermally activated, and

$$D_1^{\ell} = 2.1 \times 10^{-4} \exp[-91{,}000/(RT)], \tag{59}$$

in cm^2/s.[40] Here R is the gas constant in cal/mole·K, and T is the temperature in K. At lower temperatures, the diffusion coefficient in enhanced by irradiation,[41,42] and

$$D_1^{\ell} = 2.0 \times 10^{-29} \beta \exp(-3161/T). \tag{60}$$

In practice, the bubble-diffusion coefficient D_i^{ℓ} is limited to values less than or equal to those predicted by a modified surface-diffusion model.[21]

The empirically derived diffusivities, Eqs. 58-60, result in fission-gas bubble diffusion in the matrix slower than predicted by the theoretical model based on surface diffusion, probably because the motion of a bubble requires the nucleation of "steps."[36-39] Since grain boundaries contain natural steps, the bubble diffusivities on the grain boundaries will probably be "enhanced" and will exhibit a different temperature dependence when compared with lattice bubble diffusivities. The values of the grain-boundary fission-gas-bubble diffusivities should lie between the values for the bubble diffusivities in the lattice (as a lower limit) and the values of the bubble diffusivities calculated from the theory of surface diffusion.

Few data are available on the values of fission-gas-bubble diffusivities on grain boundaries. The grain-boundary fission-gas-bubble diffusivities[43] used in GRASS-SST (for diffusivities less than those calculated from the theory of surface diffusion and greater than those calculated using Eq. 60 are

$$D_i^g = 1.12 \times 10^{-8} \exp[-32{,}000/(1.986T)](r_1/r_i)^{1.62} (cm^2/s). \quad (61)$$

III. CALCULATIONAL PROCEDURE

A. Calculation of Bubble-size-distribution Functions

A System of coupled equations for the evolution of the fission-gas bubble-size distributions in the lattice, on dislocations, and on grain boundaries can be derived based on the models discussed above. The equations have the form

$$\dot{F}_i^\alpha = a_i^\alpha F_i^\alpha F_i^\alpha - b_i^\alpha F_i^\alpha + C_i^\alpha \quad (i = 1, \ldots, N;\ \alpha = 1, 2, 3), \tag{62}$$

where F_i^α is the number of α-type bubbles in the ith size class per unit volume, and $\alpha = 1, 2, 3$ represents the lattice, dislocation, and grain-boundary distributions, respectively, and the coefficients b_i^α and C_i^α obey functional relationships of the form

$$q_i^\alpha = q_i^\alpha(F_1^\beta, \ldots, F_{i-1}^\beta, F_i^\gamma, F_{i+1}^\beta, \ldots, F_N^\beta)$$

$\alpha = 1$: $\beta = 1, 2, 3$; $\gamma = 2, 3$;

$\alpha = 2$: $\beta = 1, 2$; $\gamma = 1$;

$\alpha = 3$: $\beta = 1, 3$; $\gamma = 1$.

In Eq. 62, a_i^α represents the rate at which α-type bubbles are lost from (grow out of) the ith size class due to coalescence with bubbles in that class; b_i^α represents the rate at which α-type bubbles are lost from the ith size class due to coalescence with bubbles in other size classes, migration out of the structural region, change in bubble type due to bubble migration processes and re-solution; C_i^α represents the rate at which bubbles are being added to the ith size class due to fission-gas generation, bubble nucleation, bubble growth resulting from bubble coalescence, migration processes, and bubble shrinkage due to gas-atom re-solution.

Figure 1 is a GRASS-SST flow chart for one annular fuel region. Usually, for modeling purposes, the fuel is divided into many annular regions. For this situation, GRASS-SST takes into account the migration of the fission gas inward from one annular region to the next as a result of a temperature gradient. Because the coefficients b_i^α and C_i^α in Eq. 62 have an explicit spatial as well as time dependence, the solution procedure exhibits a radial coupling between the various annular fuel sections. After receiving the operating conditions, such as the time step, local fuel temperatures and stresses, grain sizes and densities, the GRASS-SST subroutine calculates the bubble radii for the size classes of bubbles under consideration (the initial number of size classes is an input number) using Harrison's extrapolated equation of state for xenon[44] as well as the generalized capillary relation

$$P_i^g(T) = \frac{2\gamma}{r_i} - \sigma_H, \tag{63}$$

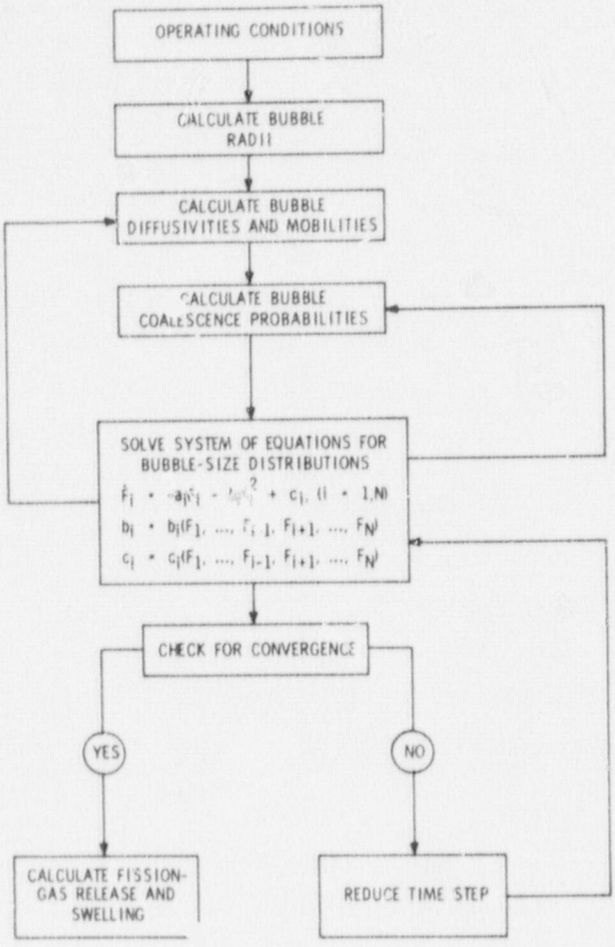

Fig. 1. GRASS-SST Flow Chart. Neg. No. MSD-62922.

where $P_i^g(T)$ is the gas pressure in a bubble with radius r_i, γ is the surface energy of UO_2, and σ_H is the local hydrostatic stress.

After the bubble radii have been determined, the bubble diffusivities, mobilities, and coalescence probabilities as well as the bubble diffusion and migration rates are calculated. The code then solves for the bubble-size distributions by using a modified midpoint rule to generate a sequence of approximations; every sequence is interpolated by rational functions to obtain a "trial" solution until specified convergence criteria are satisfied. (If required, the code will increment the number of size classes involved in the calculation.) Finally, the fission gas released and the swelling due to retained gas are calculated.

B. Fuel Swelling due to Retained Fission Gas

The intra- and intergranular swelling due to retained fission gas is calculated from the bubble-

istribution functions, F_i^α, using

$$= \frac{4}{3}\pi \sum_i r_i^3 F_i^\alpha, \tag{64}$$

ΔV_α is the total α-type bubble volume strain in the structural region sideration. The intragranular swelling strain in this region is given

$$\Delta V_{intra} = \Delta V_1 + \Delta V_2; \tag{65}$$

ΔV_3 is the total intergranular swelling strain.

The component of fuel swelling due to retained gas residing along the grain edges is computed as the difference between the volume transported by bubbles to the grain edges from the grain surfaces and the volume transported by bubbles from the grain edges to the exterior of the fuel. The volume of gas

residing along the grain edges is allowed to shrink or expand due to changes in temperature by assuming that the edge tunnels have a constant internal pressure and follow an ideal gas behavior. The total fuel swelling strain due to fission-gas bubbles (solid fission-product swelling is not included) for an axial segment of the fuel is then obtained by summing all the components of swelling strain, ΔV_α, over all the annular fuel regions k; i.e.,

$$\Delta V_{tot} = \sum_k \sum_\alpha \Delta V_\alpha . \tag{66}$$

7. Fission-gas Release

Most of the gas released from the fuel exits via the interconnected porosity reside along the grain edges (see Sec. II.F). In addition, bubbles do migrate through the fuel, and the rate at which the gas leaves any zone is included in the term b_i^α in Eq. 62. If a central hole exists in the fuel, then gas leaving the zone surrounding the central hole will be released from the fuel. The gas release rate to the central hole is given by

$$GR_{central\ hole} = A_h \sum_\alpha \sum_i F_i^\alpha v_i^\alpha S_i , \tag{67}$$

where A_h is the area of the inner boundary of the innermost fuel region, v_i^α is the average velocity of an α-type bubble (bubbles pinned to dislocations are not included), and S_i is the average number of atoms in the ith size range. The total gas release from the fuel is then given by

$$GR_{total} = GR_{interconnected\ porosity} + GR_{central\ hole} . \tag{68}$$

IV. CODE BENCHMARK

To demonstrate the degree of accuracy of the GRASS-SST solution procedure, the code was run against a classic literature problem based on a solid theoretical foundation[45] for which a rigorous numerical solution exists. Gruber[21] calculated the evolution of the lattice bubble-size-distribution function for an isothermal anneal at 1500°C, where the initial concentration of fission gas consisted only of fission-gas atoms. Gruber assumed that the gas obeyed the ideal gas law and surface diffusion was the mechanism for bubble mobility.

Before the Gruber-calculated bubble-size-distribution functions and the GRASS-SST results can be compared, the basic differences in the approaches taken must be resolved; Gruber orders the bubble sizes by the number of atoms/bubble, whereas GRASS-SST groups the bubbles into size classes, with each class characterized by an average number of atoms/bubble. If F(N)

represents the number of bubbles with N atoms per bubble and G(y) is the number of bubbles in yth size class (where m^{y-1} is the average number of atoms per bubble for bubbles in this class), then F(N) is related to G(y) by

$$F(N)dN = G(y)dy, \tag{69}$$

for

$$N = (m)^{y-1}. \tag{70}$$

Thus, the relation between Gruber's distribution function F(N) and the GRASS-SST bubble-size distribution G(y) is given by

$$F(N) = G(y)/[N\,\ell n(m)]. \tag{71}$$

Gruber presented his results in terms of reduced (dimensionless) time and with the distribution function normalized to a gas-atom concentration of 1. Figure 2 shows F(N) calculated using GRASS-SST for Gruber's conditions and with m = 2 (the GRASS-SST predictions at n = 729 were calculated with m = 3) for three successive values of the reduced time τ, where, following Gruber,

$$\tau = 91.7a_0^4 D_s f_0 (\gamma/RT)^{3/2} t, \tag{72}$$

and a_0 is the interatomic distance in centimeters, f_0 is the number of gas atoms per unit volume, t is the time in seconds, and D_s is the surface-diffusion coefficient in cm^2/s. In Fig. 2, the solid curves are fits to Gruber's results. The agreement between the GRASS-SST solution procedure and Gruber's precise numerical analysis appears to be excellent.

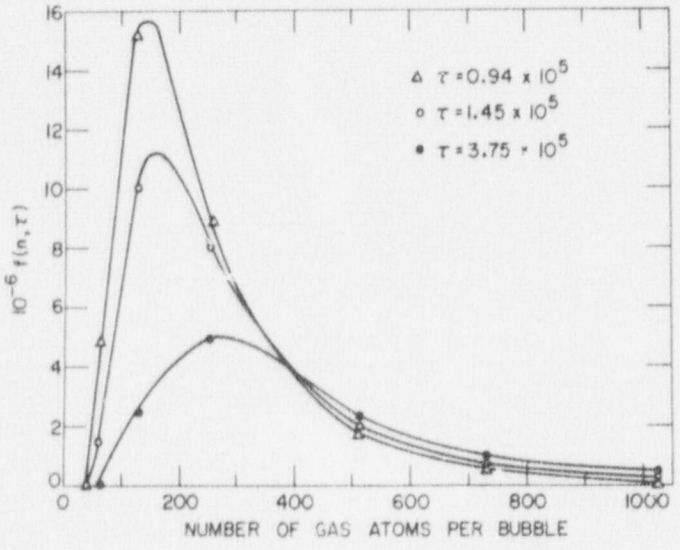

Fig. 2

GRASS-SST-calculated bubble-size Distributions as a Function of the Reduced Time τ for an Isothermal Anneal at 1500°C. The solid curves are fits to Gruber's results. Neg. No. MSD-62926.

The variation in GRASS-SST results (for Gruber's problem) with increasing m is shown in Fig. 3, where the swelling strain due to the retained fission gas is plotted against τ for m = 2 to 10. As m increases, the predicted swelling strain increases, and the difference in results between m = 2 and m = 10 is about a factor of two. However, the number of coupled equations involved in the solution procedure is a factor of three larger for m = 2 than for m = 10. Thus, the value of m used for any problem depends on an optimization between the degree of accuracy required and the length of code running time.

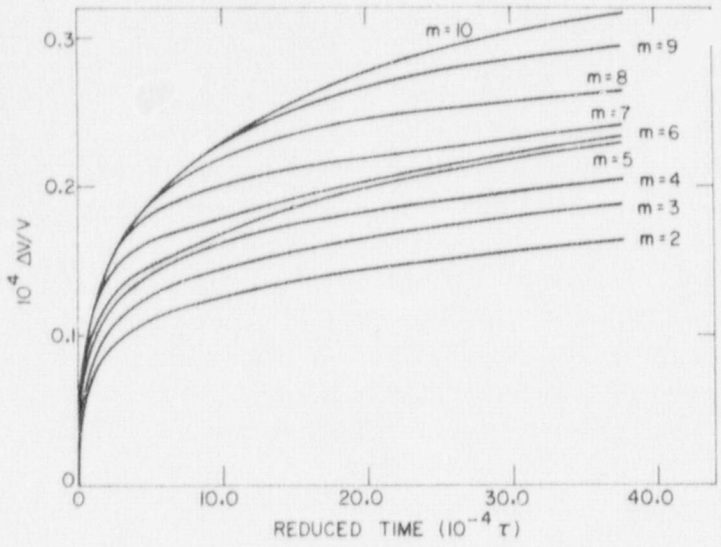

Fig. 3. Variation in GRASS-SST Strain Results for Different Values of Size Classes ($S_i = mS_{i-1}$). Neg. No. MSD-63211.

Another test of the GRASS-SST calculational procedure and the various mechanisms for fission-gas behavior incorporated in GRASS-SST is that the GRASS-SST results should reduce to the predictions of simple analytical models under specific (unrealistic) operating conditions. Figure 4 shows GRASS-SST results for the diffusion of fission gas to grain boundaries in the limit of no bubble nucleation, no coalescence, and no re-solution ($C_{ij} = b_i = 0$). This situation is not realistic, but would be comparable to low fission rates and temperatures. The solid curve is the prediction of the Booth model for gas release from a spherical grain.[12] The agreement between GRASS-SST (for these unrealistic operating conditions) and the Booth model is excellent.

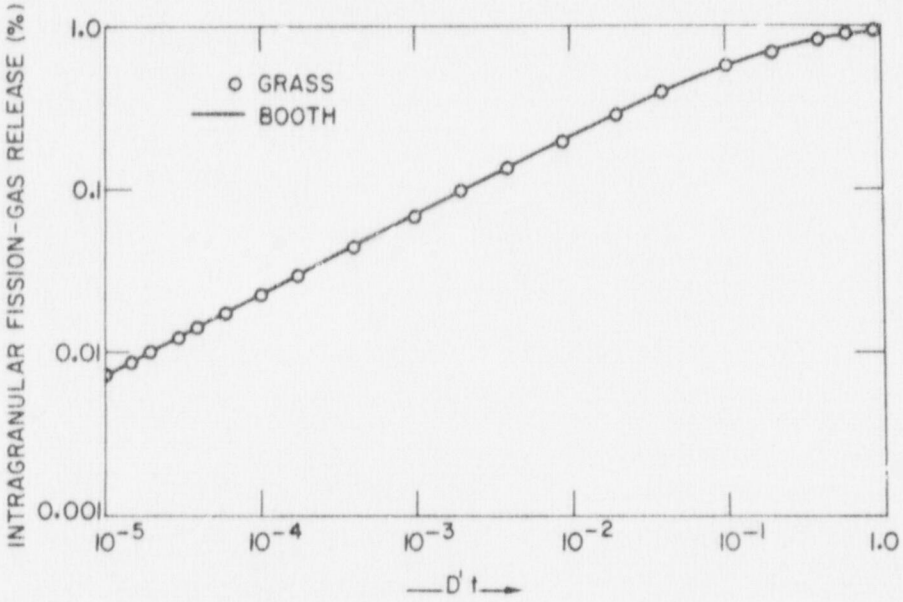

Fig. 4. GRASS-SST Results for Fractional Fission-gas Release to Grain Boundaries vs D't under Specific (Unrealistic) Operating Conditions ($D' = D_1^{\ell}/a^2$). The solid curve is the prediction of the Booth model. Neg. No. MSD-62925.

V. VERIFICATION OF GRASS-SST STEADY-STATE ANALYSIS

GRASS-SST was run using the nominal fuel-rod fabrication parameters for three steady-state irradiations in the Carolinas-Virginia Tube Reactor (CVTR), one irradiation in the H. B. Robinson No. 2 reactor, and one irradiation in the Saxton reactor. To supply GRASS-SST with the proper operating conditions for these irradiations, GRASS-SST was coupled to an LWR fuel-behavior code generated by making suitable modifications[46] to the LMFBR LIFE fuel-performance code.[2,3] GRASS-SST was coupled to the fuel-behavior code mechanically (i.e., for the calculation of the fission-gas-bubble swelling component of the total fuel swelling) as well as thermally (i.e., for the calculation of the amount of fission gas released to the fuel-cladding gap and fuel-rod plenum). Reciprocally, the LWR fuel-behavior code supplied GRASS-SST with operating conditions such as fuel temperature, state of stress, linear power, fuel density, and grain size.

Figure 5 shows the predicted versus the measured end-of-life gas release for these irradiations. The diagonal line indicates perfect agreement between GRASS-SST predictions and experiment. Table I shows the values of various parameters used in the calculation of the predicted results in Fig. 5, along with the equation number where the parameter first appears. As is evident from Fig. 5, GRASS-SST predicts the data reasonably well for fission-gas release between 1/4 and 30%, and for burnups between 0.7 and 3 at. %.

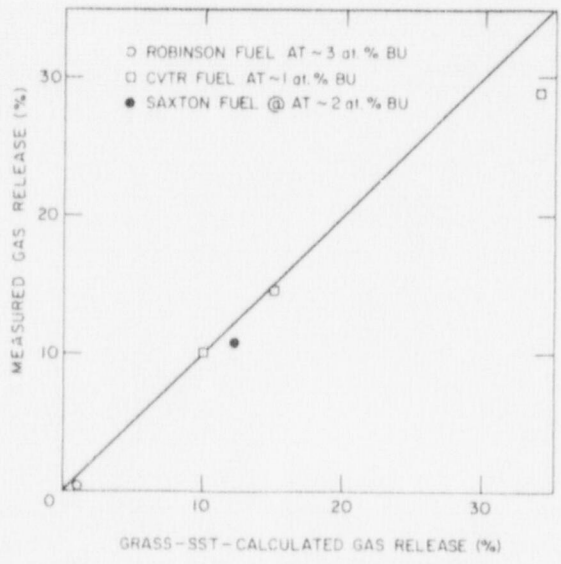

Fig. 5. Comparison of GRASS-SST Predictions with End-of-life Gas Release. Neg. No. MSD-65143.

Figure 6 shows GRASS-SST-calculated intragranular bubble density versus bubble diameter at a fractional radius of ~0.20 for the H. B. Robinson fuel at end of life. Also shown in Fig. 6 is an estimate of the measured density of fission-gas bubbles obtained from replica fractographs.[7] Bubbles having diameters less than 100 Å were below the limit of resolution and thus were not observable. The calculated bubble-size distribution, shown in Fig. 6, consists mainly of fission-gas atoms and very small (~100 Å) fission-gas bubbles. The absence of large bubbles is due to the low fuel temperatures characteristic of the H. B. Robinson irradiation, especially during the second cycle when centerline temperatures were about 900°C. From Fig. 6, the calculated bubble densities are in reasonable agreement with the data.

TABLE I. Values of Various Parameters Used in Calculating GRASS-SST-predicted Results

Parameter	Value	Defined in Eq. No.
α	0.30	1
f_N	0.9×10^{-5}	2
b_0	1×10^{-19} cm^3	17
r_d	5×10^{-6} mm	17
ρ_d	1×10^{7} mm/mm^3	18
E_v^f	2.2 eV	37
D_v^0	1 mm^2/s	38
E_v^m	2.2 eV	38
κ	1	42
δ	5×10^{-6} mm	48a
CN	4.0	55
σ	0.30	56
B_{vcrit}	0.07	57
γ	$\gamma = 1507 - 0.3459T$ ergs/cm^2[a]	63

[a]Data from Ref. 48.

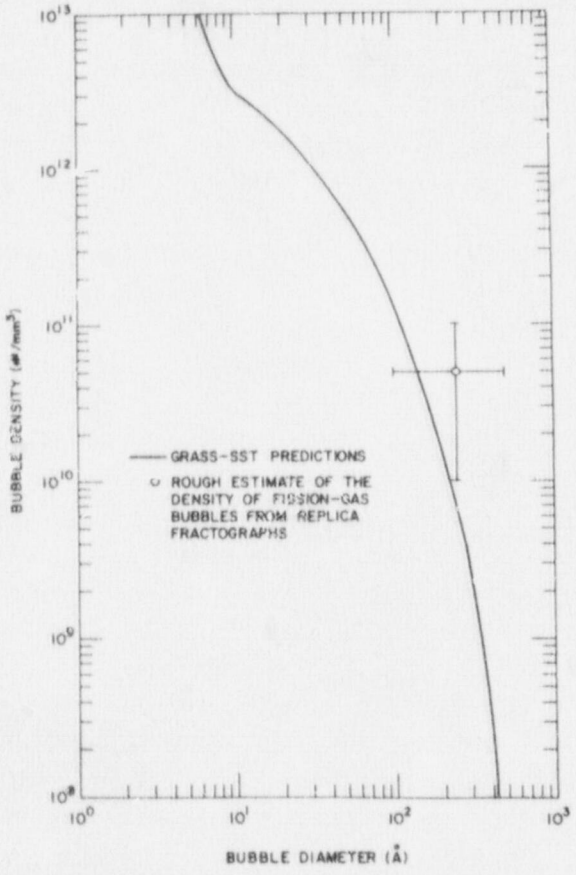

Fig. 6

GRASS-SST-calculated Intragranular Bubble Density vs Bubble Diameter for H. B. Robinson Fuel at End of Life, Compared with Experimental Data. Bubbles with diameters $\lesssim$100 Å were below the limit of resolution. Neg. No. MSD-64690.

Figure 7 shows GRASS-SST-calculated results for fuel swelling due to lattice, grain-boundary, and grain-edge fission gas versus burnup in CVTR rod 33.833. The temperature history is also recorded and illustrates the variable power levels at which the rod was operated. Despite the complicated irradiation history of this rod, one feature of fuel swelling is quite clear: At burnups ≃0.5 at. %, the grain-edge swelling begins to dominate the sum of the lattice and grain-boundary swelling contributions, and, at burnups >0.5 at. %, most of the volume increase results from the interlinked tunnels of fission gas along the grain edges. At burnups <0.5 at. %, most of the swelling is due to the lattice and grain-face bubbles.

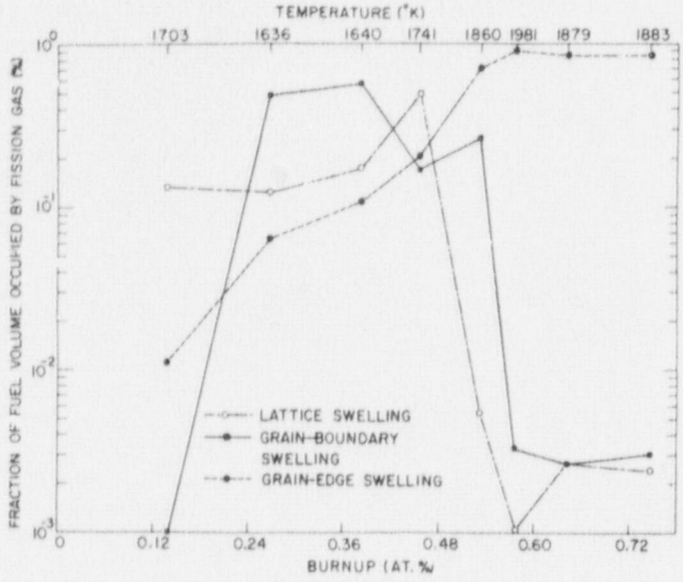

Fig. 7. GRASS-SST-calculated Lattice, Grain-boundary, and Grain-edge Swelling vs Burnup for CVTR Rod 33.833. The upper scale shows the fuel temperature that corresponds to each set of swelling results and illustrates the various fuel-rod power levels. Neg. No. M -64684.

This feature of fission-gas swelling is in qualitative agreement with the results of Turnbull and Tucker,[18] in which the grain-edge swelling in UO_2 irradiated at 1750°C dominated the grain-face swelling at ~0.42-at. % burnup. Turnbull and Tucker found that, at lower burnups (0.13 at. %), grain-face bubbles dominated the volume increase and, at a relatively medium burnup (~0.26 at. %), the grain-face and grain-edge swelling had approximately the same order of magnitude.

Figures 8 and 9 show GRASS-SST-calculated results for the radial distribution of fuel swelling and percentage of retained fission gas, respectively, at 0.78 at. % burnup in CVTR rod 33.833. The results shown in Figs. 8 and 9 indicate that most of the fuel swelling is at the center of the UO_2 rod and is due to excessive concentration of fission-gas bubbles along the grain edges. At much higher temperatures, when extensive columnar grain growth has occurred and permits many of these interlinked tunnels to vent to the fuel-rod plenum, the curve in Fig. 8, which describes the radial dependence of swelling, becomes bell-shaped and peaks at approximately the fuel midradius.[49] This behavior is typical of breeder-reactor fuel. The radial distribution of retained fission gas shown in Fig. 9 rises quite sharply from the 25% fraction of retained gas at the central region to 99% at approximately three-fourths of the fuel radius. This feature of fission-gas behavior agrees qualitatively with reported results.[49]

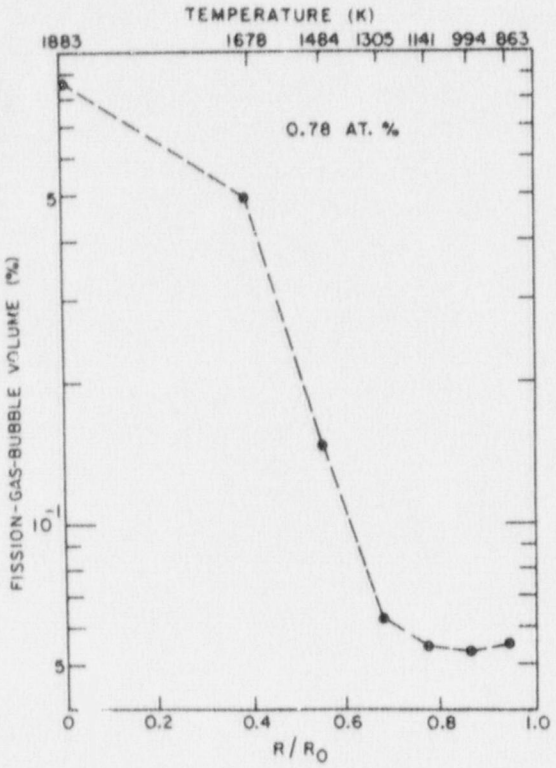

Fig. 8. GRASS-SST-calculated Swelling vs Fractional Radius for CVTR Rod 33,833. Neg. No. MSD-62658.

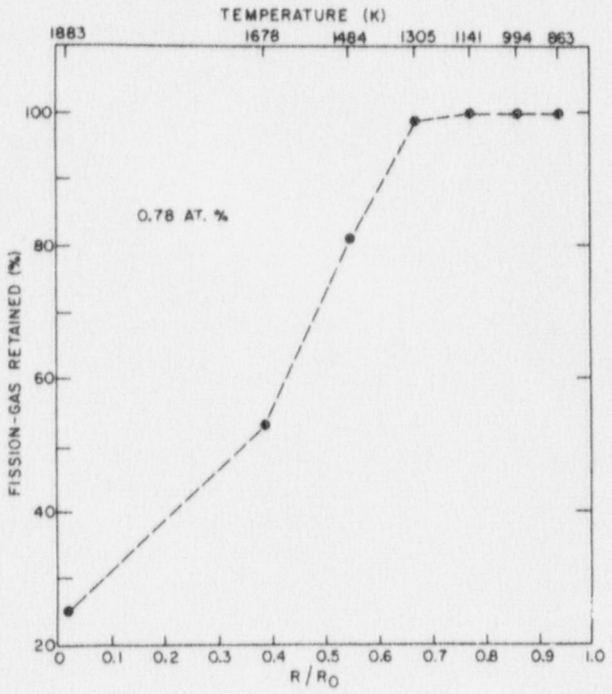

Fig. 9. GRASS-SST-calculated Fraction of Retained Fission Gas vs Fractional Radius for CVTR Rod 33,833. Neg. No. MSD-62663.

In Sec. VII, GRASS-SST verification results are presented for transient heating (DEH) tests on fuel pellets irradiated in the H. B. Robinson and Saxton reactors. The steady-state simulation establishes the initial conditions in the fuel pellet before DEH testing (e.g., bubble-size distributions and amounts and location of retained gas).

Table II shows results of the GRASS-SST steady-state simulations (see also Figs. 5 and 6) for total gas release from the rods as well as the quantity of gas retained in the pellets used for DEH testing. Also listed in Table II are the experimentally determined values for these quantities.[47] From Table II, the calculated quantities of retained gas in the pellets before DEH testing are in reasonable agreement with the data.

TABLE II. GRASS-SST-calculated Values for Total Gas Release from Saxton and H. B. Robinson Fuel Rods and for Quantity of Gas Retained in Pellets Used for DEH Testing, Compared with Experimental Results

Fuel	Total Calculated Gas Release from Rod, mm mole	Total Measured Gas Release from Rod, mm mole	Total Calculated Quantity of Gas Remaining in Fuel Pellet, μmole/g	Total Measured Quantity of Gas Remaining in Fuel Pellet, μmole/g
H. B. Robinson	0.12	0.18	36	31
Saxton	1.10	0.958	17	16

VI. STEADY-STATE SENSITIVITY ANALYSES

Information that can be used to determine the influence of individual physical models on the overall behavior of fission-gas in LWR fuels as well as to assess key factors influencing fission-gas release can be obtained through sensitivity (or parametric) analyses. Tables III and IV list the results of GRASS-SST calculations for fractional fission-gas release from UO_2 grains to the grain edges versus temperature for various values of irradiation time, grain size, fission rate, and temperature gradient. These values for the fractional fission-gas release are upper bounds on the amount of gas that would actually be released from the fuel; due to the incomplete interconnection of grain-edge tunnels within the UO_2, the amount of gas released from the fuel is usually less than that released to the grain edges.

TABLE III. GRASS-SST Calculations for Fractional Fission-gas Release from 10- and 30-μm Grains for Fission Rate of 1×10^{13} f/cm^3·s and Temperature Gradient of 200°C/cm. Neg. No. MSD-64693.

TEMPERATURE (°C)	FISSION-GAS RELEASE (%) FROM 10-μm GRAINS / FISSION-GAS RELEASE (%) FROM 30-μm GRAINS	TIME (h) 60	110	210	510	1010	2010	3010	4010	5010	6010	8010	10010	11960
1200		0.13	0.14	0.16	0.20	0.24	0.30	0.35	0.38	0.42	0.44	0.49	0.53	0.56
		0.005	0.006	0.008	0.012	0.016	0.021	0.025	0.028	0.031	0.033	0.037	0.041	0.044
1300		0.22	0.29	0.40	0.61	0.96	1.40	1.73	1.98	2.21	2.41	2.75	3.04	3.29
		0.01	0.02	0.04	0.06	0.10	0.15	0.19	0.22	0.25	0.27	0.32	0.35	0.38
1400		0.56	0.92	1.66	3.65	5.03	8.99	11.08	12.77	14.21	15.46	17.56	19.28	20.72
		0.04	0.09	0.18	0.50	0.92	1.41	1.74	2.03	2.27	2.47	2.79	3.03	3.25
1500		1.92	4.26	7.81	14.28	20.83	29.08	34.70	39.01	42.50	45.42	50.14	53.76	56.56
		0.15	0.57	1.35	2.80	4.60	5.82	6.89	7.70	8.36	8.89	9.71	10.34	10.90
1600		6.48	12.11	19.37	29.74	36.96	46.78	53.98	59.51	63.84	67.32	72.53	76.16	78.74
		0.82	2.20	4.36	7.67	10.16	13.51	15.95	17.94	19.65	21.18	23.84	26.14	28.15
1700		14.27	21.36	31.75	41.77	56.18	70.93	78.29	82.52	85.19	87.02	89.33	90.75	91.69
		2.35	4.85	7.49	13.32	19.82	28.04	33.78	38.32	42.11	45.40	50.91	55.40	59.08
1800		17.30	27.15	42.18	64.38	78.69	87.90	91.16	92.83	93.86	94.57	95.49	96.09	96.51
		4.23	7.96	14.26	25.58	36.69	50.22	59.11	65.60	70.56	74.48	80.11	83.92	86.57
1900		26.73	44.96	64.10	83.33	91.19	95.33	96.77	97.52	97.99	98.31	98.72	98.97	99.14
		6.95	14.98	25.65	43.35	59.62	76.36	84.69	89.36	92.19	94.02	96.14	97.29	97.92
2000		42.80	61.40	80.90	92.61	96.59	98.43	98.98	99.24	99.39	99.49	99.70	99.90	100
		13.30	26.15	41.25	64.67	81.60	92.85	96.30	97.73	98.44	98.83	99.20	99.35	99.43
2400		86.64	95.54	98.05	100	100	100	100	100	100	100	100	100	100
		75.31	91.98	97.26	99.29	100	100	100	100	100	100	100	100	100

TABLE IV. GRASS-SST Calculations for Fractional Fission-gas Release from 10-μm Grains for Fission Rate of 1.3×10^{12} f/cm^3·s for Two Values of Temperature Gradient. Neg. No. MSD-64694.

TEMPERATURE (°C)	FISSION-GAS RELEASE (%) WITH A 200° C/cm TEMP. GRADIENT / FISSION-GAS RELEASE (%) WITH A 1000°C/cm TEMP. GRADIENT	TIME (h) 110	210	310	510	1010	2010	3010	4010	5010	5910
1200		0.29	0.32	0.34	0.39	0.46	0.55	0.64	0.73	0.82	0.89
		0.30	0.36	0.42	0.54	0.80	1.11	1.39	1.66	1.91	2.13
1300		0.65	0.86	1.09	1.41	1.98	3.08	4.02	4.83	5.55	6.14
		0.88	1.44	1.97	2.89	4.51	6.20	7.76	9.07	10.22	11.15
1400		1.59	2.54	3.39	5.12	9.19	13.49	17.09	20.02	22.52	24.51
		2.76	4.62	6.07	8.31	12.21	17.49	21.27	24.39	27.06	29.19
1500		3.78	8.31	11.89	16.56	24.56	34.58	41.54	46.88	51.24	54.57
		6.92	10.97	13.93	18.91	26.48	36.04	42.63	47.71	51.85	55.00
1600		10.21	20.03	25.78	33.62	44.26	53.28	59.33	64.39	68.57	71.70
		14.73	22.18	28.09	34.93	43.26	51.39	57.96	63.47	67.97	71.32
1700		23.34	32.46	35.41	39.31	51.21	68.86	77.96	83.12	86.36	88.36
		26.35	33.31	35.46	39.24	51.95	70.35	79.85	85.21	88.54	90.58
1800		24.39	28.78	36.94	53.58	74.21	87.03	91.46	93.68	95.02	95.83
		23.14	28.64	38.82	56.29	77.78	90.74	94.90	96.80	97.82	98.38
1900		24.70	44.80	61.07	76.82	89.44	95.58	97.55	98.27	98.72	98.98
		27.52	51.98	69.20	85.02	95.26	98.60	99.33	99.60	99.72	99.77
2000		39.86	68.75	80.37	89.79	96.37	98.85	99.38	99.57	99.66	99.72
		53.09	82.77	92.16	97.39	99.32	99.73	99.82	99.87	99.89	99.91
2400		97.63	99.73	99.92	99.96	99.98	100	100	100	100	100
		100	100	100	100	100	100	100	100	100	100

The following observations can be derived from the results of this analysis:

1. The fractional fission-gas release has a strong dependence on temperature. Figure 10 shows the fractional fission-gas release as a function of temperature for various values of the fuel burnup calculated from Table III.

2. The fractional fission-gas release is time-dependent. The rate of gas release depends on the irradiation time as well as on the temperature. In all cases, the fractional gas release increases with the time.

3. The fractional fission-gas release has a strong dependence on the UO_2 grain size. The rate of fission-gas release increases as the UO_2 grain size decreases. For example, Fig. 11 shows the fractional fission-gas release from 10- and 30-μm grains as a function of temperature for two values of the

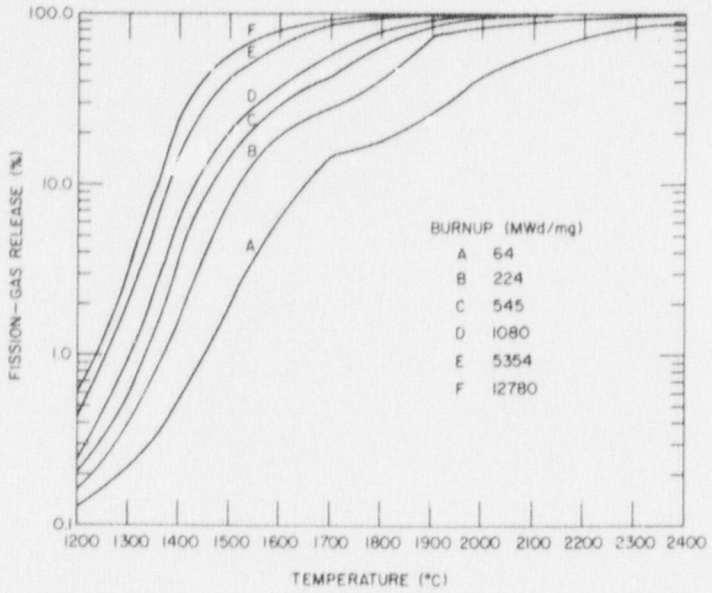

Fig. 10. GRASS-SST-calculated Fission-gas Release as a Function of Fuel Temperature and Burnup from 10-μm Grains with 200°C/cm Radial Temperature Gradient. ANL Neg. No. 306-77-131.

fuel burnup. These results agree with recent experiments in which fission-gas release from UO_2 pellets irradiated at 1750°C decreased significantly with increasing grain size.[50]

4. The fractional fission-gas release has a moderate dependence on the temperature gradient. The rate of fission-gas release increases as the temperature gradient increases.

5. The fractional fission-gas release has a strong dependence on the degree of interconnection of grain-edge tunnels. Due to the incomplete interconnection of the grain-edge tunnels, the amount of gas actually released from the fuel will be less than the amount released to the grain edges. In general, the degree of tunnel interconnection depends on the fuel microstructure (e.g., grain size, UO_2 density, and fabricated pore-size distribution) and hence is a function of the irradiation time.

Fig. 11

GRASS-SST-calculated Fission-gas Release from 10- and 30-μm Grains as a Function of Fuel Temperature with 200°C/cm Radial Temperature Gradient for Two Values of Burnup. ANL Neg. No. 306-77-357.

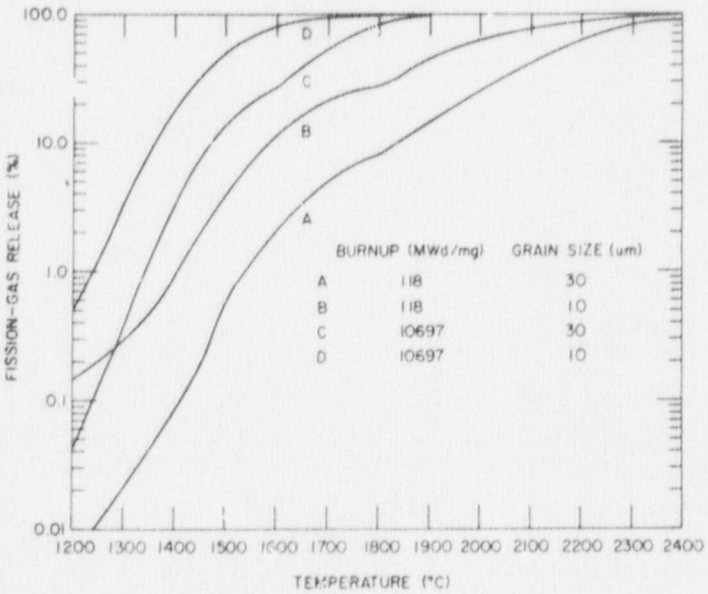

Intragranular gas-bubble diffusivities and gas-atom re-solution rates in UO_2 are materials properties that can strongly affect intragranular gas release during steady-state conditions. Estimates of the diffusivity of atomic

xenon at 1500°C, based on the results of various experiments,[34] differ by as much as three orders of magnitude. Gas-atom re-solution rates are extremely difficult to obtain experimentally, and theoretical estimates are very model-dependent. Figures 12 and 13 show the calculated end-of-life values for the fraction of fission gas reaching the grain edges for the H. B. Robinson fuel as a function of the intragranular gas-bubble diffusivity and gas-atom re-solution rate, respectively. These results were generated assuming that the fraction, F_{BL}, of the gas atoms knocked out of grain-boundary bubbles due to re-solution which reenter the lattice equals 1.0.

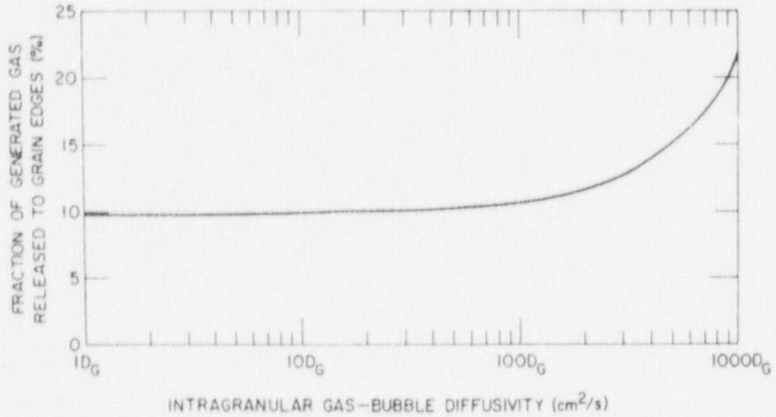

Fig. 12

GRASS-SST-calculated Fraction of Fission Gas Reaching Grain Edges as a Function of Intragranular Bubble Diffusivity for F_{BL} = 1.0. Neg. No. MSD-65138.

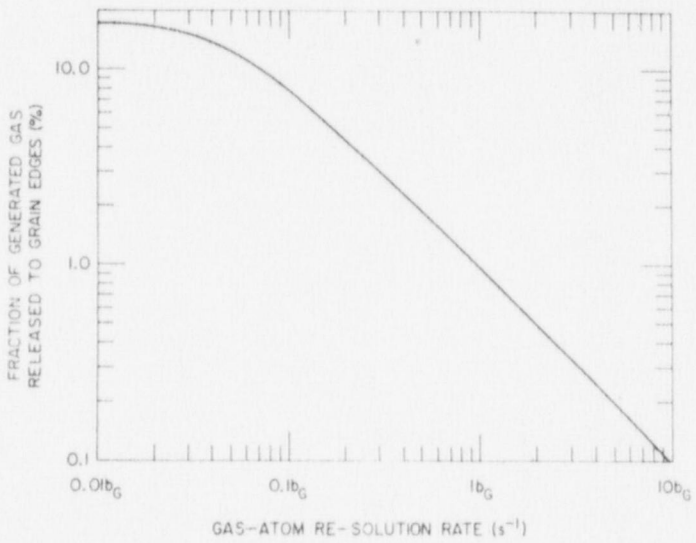

Fig. 13

GRASS-SST-calculated Fraction of Fission Gas Reaching Grain Edges as a Function of Gas-atom Re-solution Rate for F_{BL} = 1.0. Neg. No. MSD-64141.

Figures 12 and 13 show that intragranular gas release increases as the diffusivities increase and the re-solution rate decreases. The intragranular gas release increases as the re-solution rate decreases due to a corresponding decrease in the flux of "re-solution" atoms from the boundaries back to the lattice. However, the assumption that all gas atoms leaving grain-boundary bubbles due to re-solution reenter the lattice (i.e., F_{BL} = 1.0) may not be realistic. Some of the gas atoms knocked out of grain-boundary bubbles may remain on the boundaries, or stop close enough to the boundaries to be quickly recaptured.

Figures 14 and 15 show the calculated end-of-life values for the fraction of fission gas reaching the grain edges for the H. B. Robinson fuel for various values of the intragranular gas-bubble diffusivities and the gas-atom re-solution rates, respectively, assuming that none, i.e., $F_{BL} = 0$, of the gas atoms leaving the boundaries due to re-solution reenter the lattice. Figure 15 shows that intragranular gas release increases as the re-solution rate increases. Figure 14 shows that intragranular gas release is relatively insensitive to changes in the intragranular fission-gas bubble diffusivities. These results show that, for $F_{BL} = 0$, intragranular gas release is re-solution controlled; i.e., the gas released from the grains consists mainly of single gas atoms. Fission-gas bubbles behave primarily as temporary gas-atom trapping sites.

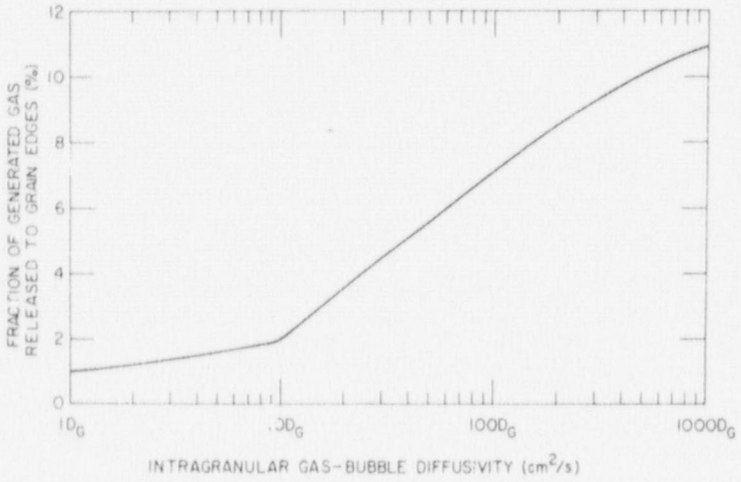

Fig. 14

GRASS-SST-calculated Fraction of Fission Gas Reaching Grain Edges as a Function of Intragranular Bubble Diffusivity for $F_{BL} = 0$. Neg. No. MSD-65140.

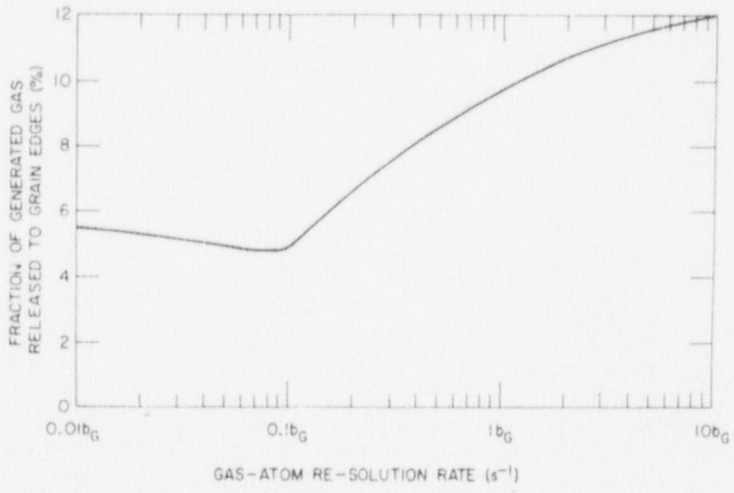

Fig. 15

GRASS-SST-calculated Fraction of Fission Gas Reaching Grain Edges as a Function of Gas-atom Re-solution Rate for $F_{BL} = 0$. Neg. No. MSD-65139.

The GRASS-SST-calculated behavior of intragranular fission-gas release as a function of the intragranular bubble diffusivities and of the gas-atom re-solution rates for $F_{BL} = 0$ described above agrees with the theoretical predictions of Speight[51] and others.[52] The value of the gas-atom re-solution rate calculated using Eq. 17 (see Table I for the values of the corresponding parameters) for a fission rate of 8.5×10^{18} f/m^3·s is

$b_1 \simeq 1 \times 10^{-6}$/s compared to an upper limit established by Turnbull and Cornell[53] of $b_1 \leq 10^{-5}$/s. Although the value of the gas-atom re-solution rate, b_1, used in GRASS-SST is consistent with this upper limit, $b_1 \simeq 10^{-6}$/s is smaller than most values previously reported.[54] The values of the parameters used in Eq. 17 (i.e., b_0 and r_d; see Table I) were selected to obtain the best agreement between GRASS-SST predictions and experiment for both steady-state irradiations (see Sec. V) and transient heating conditions (see Sec. VII.E).

VII. VERIFICATION OF GRASS-SST TRANSIENT ANALYSES

A. Experimental Support

The DEH experiments[5,7,8] were performed on two fuel types with different irradiation histories. Most of the experiments were performed on commercial pressurized-water-reactor (PWR) fuel obtained from the H. B. Robinson No. 2 reactor. Fuel from rods F7 and G6 of assembly BO5 were used in the present study. This fuel was irradiated to a peak burnup of 3.14 at. % in two reactor cycles at peak linear heat-generation rates (LHGR's) of 22.4 and 17.7 kW/m, respectively.[7] The axial power profiles for the rods contained broad plateaus that extended over the central ~2.5 m of the 3.7-m fuel regions.[55] The rod-averaged fission-gas release during the Robinson irradiation was ~0.2% of the amount generated (see Fig. 5).[56] The low gas release is indicative of low operating temperatures.

One DEH experiment was performed on a specimen taken from an experimental load-follower rod irradiated in the Saxton PWR. This rod, No. 843, experienced peak LHGR's of ~50 kW/m for short periods during its irradiation.[57] Pronounced axial power peaking also occurred. At the axial level from which the DEH test specimen was obtained, the time-averaged LHGR was ~36 kW/m.[57] The rod-averaged fission-gas release for rod 843 was 8.5% (see Fig. 5).[47]

In the transient heating tests, ohmic heating of the fuel by the DEH technique,[58,59] with cooling provided by a helium stream, produced temperature profiles similar to those that occur during reactor operation. After steady-state temperatures were achieved, the power was increased in a programmed manner to produce transient heating of the fuel. Temperature profiles during the test were calculated on the basis of material properties of UO_2 and experimentally measured parameters such as power input and fuel surface temperatures. The calculated temperature profiles have been verified by their prediction of centerline melting of the irradiated fuel.[5,7]

Posttest examinations of the fuel were made to assess the changes in the fuel that were due to transient heating. The most striking features revealed in polished sections of the fuel were the appearance of cracks in the

form of intergranular separations within the fuel. This pattern of cracks can be seen in Fig. 16, a high-magnification view of a transverse section of transient-heated fuel.[4,5,7] Experimental results[5,7] indicate that intergranular separations can form by the diffusion-controlled processes of growth and coalescence of fission-gas bubbles.

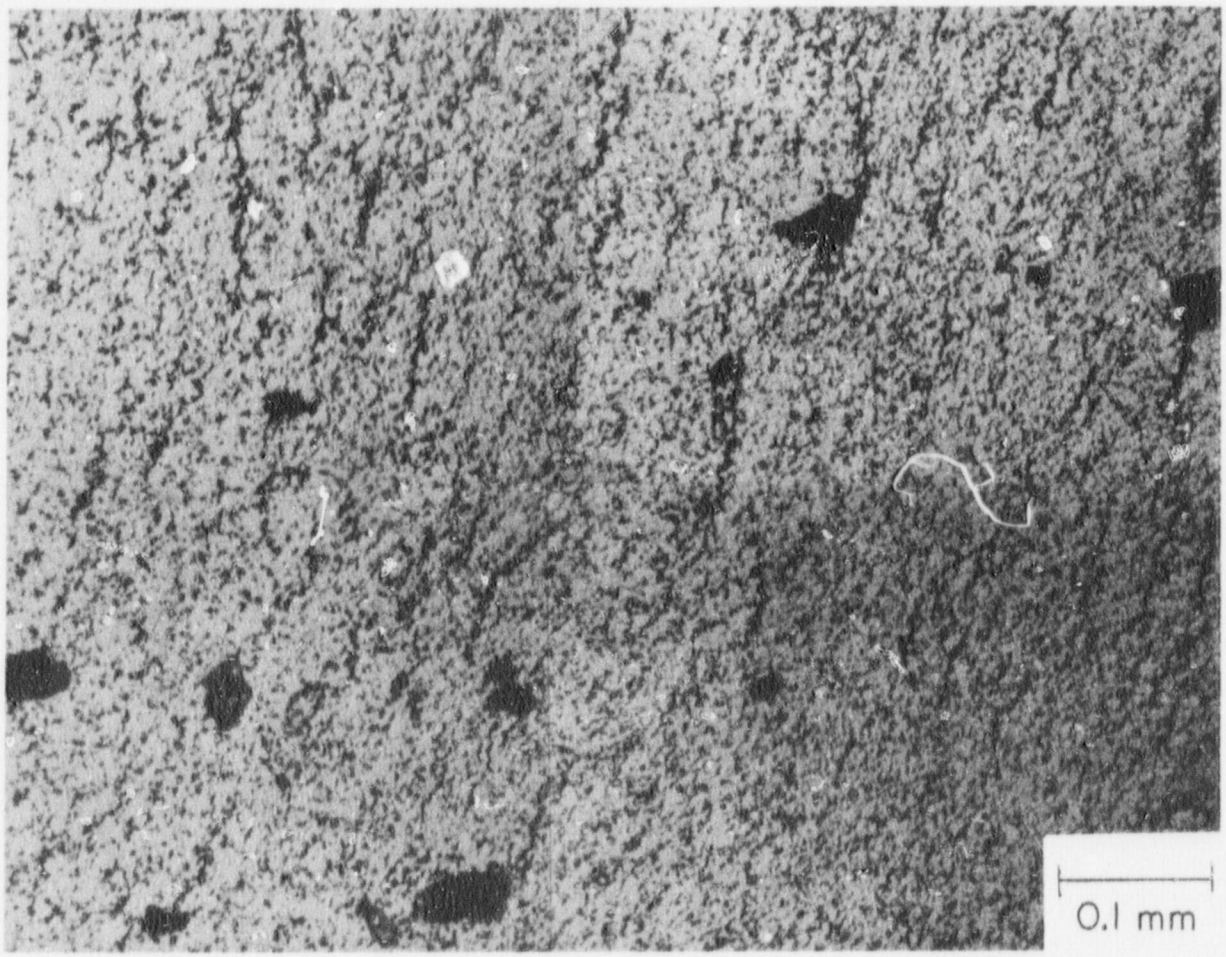

Fig. 16. Optical Micrograph of Transient-heated Fuel Showing Separations Caused by Motion at Grain Boundaries. The motion was in response to stresses from, for example, gas pressure and fuel-end loading. From Ref. 4. Neg. No. MSD-187873.

In addition, this gradual process of bubble growth and coalescence to form channels and channel coalescence to form separations can be interrupted by the more rapid process of crack propagation. Crack propagation results from stresses on weakened grain boundaries. The stresses responsible for cracking are the result of the applied axial load, differential thermal expansion, and the pressurization of intergranular fission-gas bubbles. Separations covering up to 80% of the fuel volume have been observed in UO_2 pellets after DEH testing and thus may have provided an important release mechanism for fission gas that had moved out of the grains of the irradiated fuel.[5-8]

The model development and verification of the transient portion of GRASS-SST are based on the results of 11 PCM-type DEH tests.[8] Figure 17, a plot of xenon release as a function of total energy for these DEH tests, shows that there is a general trend of higher gas-release fractions at higher total power depositions. Test 31 shows the only large deviation from the trend indicated by the parallel dashed lines in Fig. 17. This deviation may be due to the long, high-power pre-transient heating in test 31. Tests 21, 26, and 33 were run to produce small melt fractions. The gas release from the small amount of molten fuel has been shown in all cases to be small compared to the release from the unmelted region.[7] Fuel melting did not occur for the other tests listed in Fig. 17.

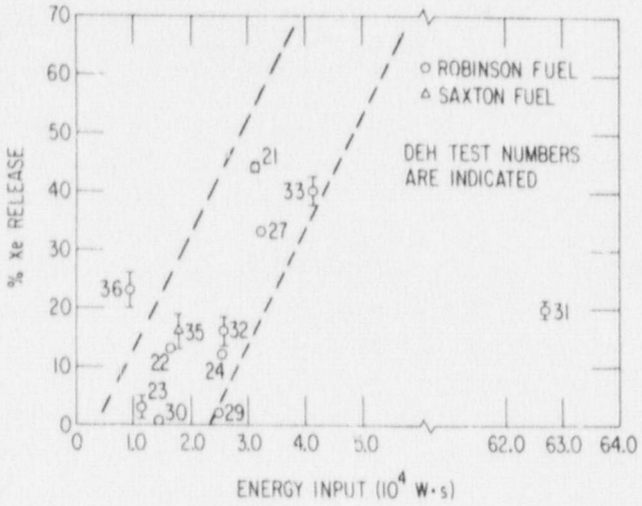

Fig. 17. Percent Xenon Release vs Energy Input for DEH-tested Specimens (from Ref. 8). Neg. No. MSD-64912.

Transient temperature histories of the DEH tests are calculated with the DEH Transient Temperature Distribution (DEHTTD) code.[60] The transient heat-transfer equation is solved by this code, which accepts measured values of current, voltage, and surface temperature as input and uses expressions taken from the literature for the thermal and electrical conductivities of UO_2.

For use in the present study, a model[8] for the effect of intergranular separations on heat transfer was included in the DEHTTD code. These separations form during transient heating and reduce the effective thermal conductivity of the fuel. In the DEHTTD code, the separations are assumed to form linearly with time, and the reduction in thermal conductivity is assumed to be proportional to the extent of the separations, as measured by their specific surface area. That is, the code uses a thermal-conductivity expression of the form

$$T_K' = (1 - F)T_K, \tag{73}$$

where T_K' is the effective thermal conductivity, F is the cracking factor (so called because the separations often resemble cracks), and T_K is the temperature-dependent thermal-conductivity expression of Washington.[61] The cracking factor, F, was assumed to equal zero at the start of transient heating and to increase linearly with time to a maximum value, which occurred at maximum power, given by

$$F_{max} = 1.55 \times 10^{-3} S_V^{\alpha P}, \quad (74)$$

where $S_V^{\alpha P}$ is the posttest value of pore-solid surface area per unit volume in units of mm^{-1}.

B. Effect of Transient Heating on Intragranular Fission-gas Bubbles

Analyses with GRASS-SST for steady state conditions, coupled with experimentally determined fission-gas release during DEH tests, indicate that large quantities of gas are being transported out of the UO_2 grains during transient heating. This release of fission gas from the grains is much greater than can be explained by means of empirical steady-state diffusivities. In addition, analyses for transient-heating conditions indicate that GRASS-SST can account for the rapid diffusion of fission gas out of the UO_2 grains during DEH tests if the high-temperature bubble mobilities are enhanced due to an increased rate of atom attachment to and detachment from the bubble surface.

The physical basis behind this approach is as follows. During equilibrium conditions, the bubbles may be faceted, and the rate of motion of a faceted bubble is determined by the frequency of nucleation of steps instead of the time required for atoms to move from a step on one side of a bubble to a step on the other side. (That is, the atom attachment and detachment rate is slower than predicted by surface diffusion.)[36-39,63] However, if the atom attachment and the detachment rate increased during transient conditions, higher bubble diffusivities would result.

Recrystallization and dislocation sweeping are other phenomena that could, in principle, result in an enhanced release of fission gas from the grains to the grain boundaries during transient-heating conditions. Observations of the DEH-tested pellets reveal no evidence of UO_2 recrystallization.[62] GRASS-SST analyses indicate that a rapid diffusion of fission-gas bubbles (~100 Å in diameter) as well as of gas atoms occurs during the DEH transient heating. Dislocation sweeping could conceivably move fission-gas atoms from the grains to the grain boundaries, but is unlikely to have much effect on fission-gas bubbles; the bubbles would act as pinning sites and retard the motion of dislocations. On the other hand, a rapid increase in the atom attachment and detachment rate would lead to increased bubble mobility for small as well as large bubbles.

C. Mobility of Overpressurized Fission-gas Bubbles

Bubbles intersected by dislocations have higher diffusivities than bubbles in a perfect lattice.[64] The bubble diffusivities were satisfactorily described by a rate-controlling nucleation mechanism, in which ledges introduced into the bubble surface by the dislocation rotated about the dislocation, causing the bubble to migrate. Since dislocations may extend to the grain surfaces, they can serve as channels that facilitate the migration of the bubbles

out of the grains to the grain boundaries. During steady-state heating, the dislocation density is relatively small, and the effective diffusivities of the intragranular bubbles would not be expected to be appreciably altered.

However, during transient heating, differential thermal expansion and external loads can increase dislocation densities. The stress field around an overpressurized bubble can lead to additional increases in the dislocation density near the bubble. Overpressurization is due to a lack of vacancies in a lattice that is not in thermodynamic equilibrium. If the overpressure in a bubble results in an equivalent stress that exceeds the yield strength of the UO_2, then plastic deformation of the material around the bubble will result. Since the bubble surface intersects the resultant dislocations, ledges are produced that can facilitate atom attachment and detachment.

Since plastic deformation of the UO_2 due to an overpressurized bubble is expected to result in a high density of dislocations around the bubble surface, the diffusivity of such a bubble would be expected to increase rapidly. In effect, bubble diffusion would depend more on the time required for atoms to move from a step on one side of a bubble to a step on the other (i.e., surface diffusion) than on the frequency of nucleation of steps.

As the lattice approaches thermodynamic equilibrium, the bubbles expand at a faster rate as a result of the availability of lattice vacancies and lose their overpressurization. When the material around a bubble is no longer undergoing plastic deformation, the dislocations quickly anneal out. Under these conditions, bubble mobility is quickly reduced as the diffusion of the bubbles becomes once again dominated by the frequency of step nucleation.

D. Model for Diffusion of Overpressurized Fission-gas Bubbles

To quantify the ideas presented in Sec. VII.C, consider the excess internal gas pressure in a bubble of radius r_i given by

$$P_i^{ex} = P_i^g(T) - \frac{2\gamma}{r_i}, \tag{75}$$

where γ is the effective surface tension, and

$$P_i^g(T) = 3n_i kT/(4\pi r_i^3 - 3b_v n_i) \tag{76}$$

is the gas pressure within the bubble at temperature T. Equation 76 is a rearrangement of the Van der Waals equation; $b_v = 8.3 \times 10^{-23}$ is Van der Waals constant for xenon/krypton, k is the Boltzmann constant, n_i is the number of gas atoms in the bubble of radius r_i, and P_i^{ex} is a measure of the resultant pressure in the matrix, which vanishes under the initial equilibrium conditions. In Eq. 75, the effect of external stresses has been neglected. Consider a time

interval, Δt seconds, of the transient during which the fuel temperatures are increasing at a rate dT/dt (°C/s). During this time, bubble coalescence and re-solution are assumed not to occur and n_i is constant and given by the initial equilibrium conditions

$$n_i = \tfrac{8}{3}\pi\gamma r_i^3/(kT_1 r_i + 2\gamma b_v), \tag{77}$$

where T_1 is the temperature at the beginning of the time interval Δt.

First consider the case in which the bubble radius, r_i, is constant over the time interval Δt. The time τ_i^y required for the bubble to obtain an excess pressure sufficient to generate an equivalent stress equal to the yield stress, σ_y, of the surrounding matrix is, using Eqs. 75 and 76, given by

$$\tau_i^y = \left[\frac{\left(\frac{2\gamma}{r_i} + \frac{2\sigma_y}{3}\right)\left(4\pi r_i^3 - 3b_v n_i\right)}{2n_i k} - T_1\right] \Bigg/ \frac{dT}{dt}, \tag{78}$$

where $\sigma_y = \sigma_y(T)$ is used to emphasize that σ_y is a strong function of the fuel temperature. Equation 78 does not take into account the situation in which the bubble may be overpressurized before the beginning of the time interval Δt. If the bubble was initially in an overpressurized state, then Eq. 78 would overestimate the time required for the equivalent stress generated by the overpressurized bubble to become equal to σ_y. On the other hand, if appreciable bubble relaxation occurs during time τ_i^y (i.e., r_i increases), then Eq. 78 would underestimate the time required for the equivalent stress generated by the overpressurized bubble to become equal to σ_y.

A rigorous approach to the calculation of the excess internal gas pressure for each bubble of radius r_i, where i varies over the limits of the bubble-size distribution, requires the numerical solution of a large set of coupled partial differential equations for the rate of change of bubble radii and the rate of change of the lattice-vacancy concentration, c_v.[29] Because of code-running-time requirements, this approach is outside the scope of GRASS-SST. However a phenomenological approach to the problem of bubble overpressurization can be formulated by evaluating τ_i^y as given by Eq. 78 with respect to the bubble-relaxation time, τ_i^B.

Let α_i, $0 \le \alpha_i \le 1$, characterize the degree of nonequilibrium in the lattice surrounding a bubble of radius r_i; the larger α_i, the further the system is from an equilibrium configuration. The change in α_i can be written in terms of α_i and times τ_i^B and τ_i^y (i.e., see Eq. 41 and 78) as

$$d\alpha_i = (1 - \alpha_i)d\left(\tau_i^B/\tau_i^y\right). \tag{79}$$

Thus, as τ_i^y decreases and τ_i^B increases, the system departs more from its equilibrium configuration. Conversely, as τ_i^y increases and τ_i^B decreases, the system approaches equilibrium. Solving Eq. 79 for α_i gives

$$\alpha_i = 1.0 - \exp\left(-\tau_i^B/\tau_i^y\right). \tag{80}$$

The problem that remains is to relate α_i to the bubble diffusivity. This can be accomplished by considering the limits of the bubble diffusivities used in GRASS-SST. During steady-state conditions (i.e., $\alpha_i \ll 1$), GRASS-SST uses empirical intragranular diffusivities given by (see Eqs. 58 and 59)

$$D_i^{\ell} = 2.1 \times 10^{-4} \exp(-91{,}000/kT)(r_i/r_1)^{1.62}. \tag{81}$$

The diffusivity of a bubble moving by surface diffusion is given by

$$D_i^s = 2.42 \times 10^{-25} \exp(-108{,}000/kT)/r_i^4. \tag{82}$$

Based on the discussions above, the bubble diffusivities during transient heating conditions should be given by Eq. 82 as $\alpha \to 1$. Thus, using Eqs. 81 and 82, we can express the fission-gas-bubble diffusivities in terms of the equilibrium parameter, α_i, as

$$D_i = \frac{6.732 \times 10^{-11} \exp[-(91{,}000 + 17{,}000\alpha_i)/kT]}{(4084 r_i)^{1.62+2.38\alpha_i}}, \tag{83}$$

where r_1 of Eq. 81 is assumed to have the value of 0.24×10^{-7} cm. When $\alpha_i \to 0$, Eq. 83 $\to$ Eq. 81, and when $\alpha_i \to 1$, Eq. 83 $\to$ Eq. 82. For intermediate values of α_i, the diffusivities given by Eq. 83 lie in between those given by Eq. 81 as a lower limit and those given by Eq. 82 as an upper limit.

To use Eq. 83, the UO_2 yield stress, σ_y, in Eq. 78 must be determined. In general, σ_y is a complex function of fuel temperature, strain rate, and microstructure (e.g., UO_2 grain size). Experiments designed to measure the UO_2 yield stress under steady-state and transient in-reactor conditions are difficult to perform, and adequate data are lacking. The UO_2 yield stress used in the calculation of gas-bubble diffusivities, as given by Eq. 83, has been determined based on the data of Roberts.[65] Roberts conducted conventional load-versus-deflection, strain-rate-change, and stress-relaxation tests on UO_2-20 wt % PuO_2 specimens in the strain-rate range of 0.1-0.4 h^{-1} and in the temperature range 1500-1800 C. The specimens, prepared from mechanically blended powders with grain sizes of 2-14.5 μm, were deformed in four-point bending in a high-temperature, inert-atmosphere furnace. The most significant observations from these experiments are the strong temperature dependence of the flow stress (flow stress decreases as the temperature increases) and the increase in flow stress with an increase in grain size. (In these experiments, the flow stress corresponds to the proportional elastic limit stress.)

An analytical expression for the yield stress as a function of the temperature and grain size was obtained from Roberts' data by quadratic regression analysis. Explicitly, for σ_y (in dynes/cm^2),

$$\sigma_y = 9.8 \times 10^5 \exp(a_0 + a_1/T + a_2/T^2), \quad (84)$$

where

$$a_0 = -179.1 + 7.0d + 0.2d^2,$$

$$a_1 = 6.5 \times 10^5 - 2.3 \times 10^4 d - 8.6 \times 10^2 d^2,$$

and

$$a_2 = -5.8 \times 10^8 + 1.8 \times 10^7 d + 8.9 \times 10^5 d^2.$$

Equation 84 is assumed valid for temperatures between 1500 and 2100°C and for grain sizes between d = 2.0 and d = 14.5 μm.

E. Comparison of Code Predictions for Transient Gas Release with Experimental Results

Figure 18 compares the results of GRASS-SST calculations of transient gas release with the measured results from the DEH tests shown in Fig. 17. The diagonal line indicates the position of perfect agreement between GRASS-SST predictions and experiment. The calculated results in Fig. 18 were made using Eq. 83. As is evident, the GRASS-SST predictions are in good agreement with the experimental measurements. Using diffusivities obtained by setting $\alpha_i = 0$ in Eq. 83, i.e., using the empirical diffusivities given by Eq. 81, the code significantly underpredicts the data for transient gas release >5%, except for test 31 for which the data are overpredicted by about a factor of two.

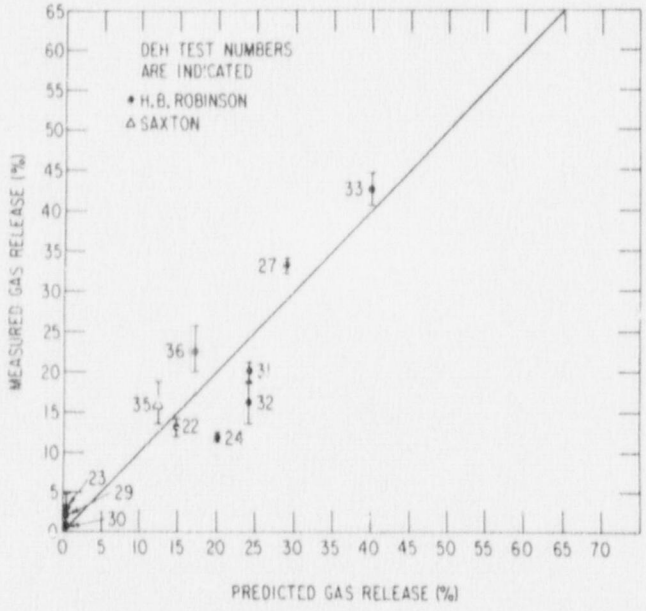

Fig. 18. GRASS-SST-predicted Transient Gas Release Using Eq. 83 vs Experimentally Measured Values. Neg. No. MSD-64915.

The fact that GRASS-SST can predict the DEH transient gas release for all DEH tests, including test 31, supports the hypothesis described in Sec. VII.D (i.e., the mobility of fission-gas bubbles is enhanced when the bubble is overpressurized, if the equivalent stress generated as a result of the excess pressure in the bubble exceeds the yield strength of the surrounding matrix).

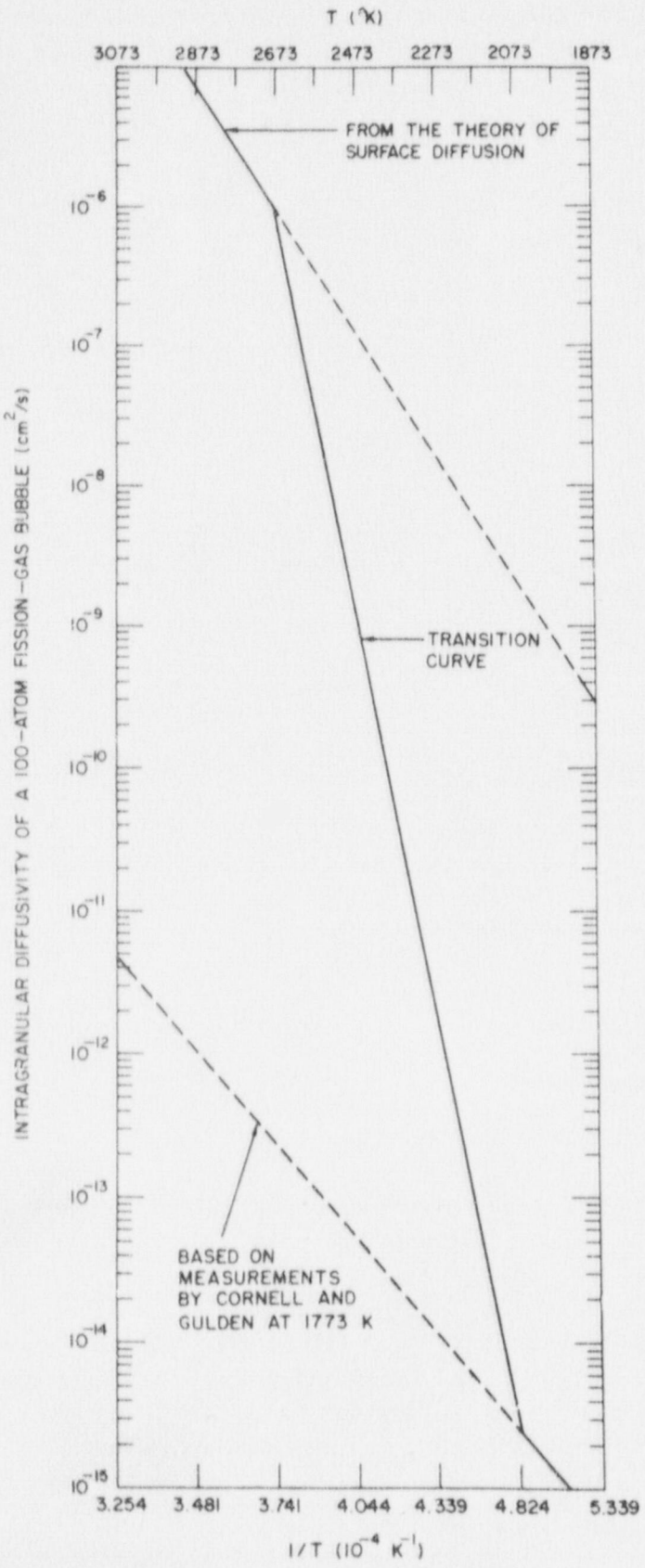

Fig. 19. Intragranular Diffusivity of a 100-atom Fission-gas Bubble as a Function of 1/T, Assuming a Temperature-dependent Transition Curve with No Dependence on Heating Rate. Neg. No. MSD-64696.

An additional demonstration of the need to model the effect that transient heating has on bubble mobility is given by the following example. Suppose the capability of GRASS-SST to predict DEH transient gas release depends only upon a relationship between the bubble mobilities and the transient temperature, and not on other parameters such as heating rate and UO_2 yield strength. For this case, the bubble diffusivities during transient heating could be described by the curve shown in Fig. 19. In Fig. 19, a transition curve starts at some critical temperature, T_c, and connects the steady-state diffusivities with those given by the theory of surface diffusion.

Figure 20 compares the results, using the bubble diffusivities shown in Fig. 19, of GRASS-SST calculations of transient gas release, with the measured results for the DEH tests shown in Fig. 17. Except for tests 24, 31, and 32, the GRASS-SST predictions (Fig. 20) based on the diffusivities shown in Fig. 19 are in reasonable agreement with much of the data. The predictions for transient gas release from tests 24, 31, and 32 are off by more than a factor of two. (Test 35 was not run for this case.) The reason for this overprediction of transient gas release is that the diffusivities shown in Fig. 19 describe enhanced diffusion of gas bubbles, even during periods when the heating rate is relatively low.

This relatively low rate of heating is characterized by test 31, which had a long steady-state preheat at high power. The

analysis leading to Eq. 83 accounts for the dependence of bubble mobility on heating rate and, as is evident from Fig. 18, predicts transient gas release in good agreement with the measured values for all the data. As other DEH test results become available, the validity of Eq. 83 will continue to be examined.

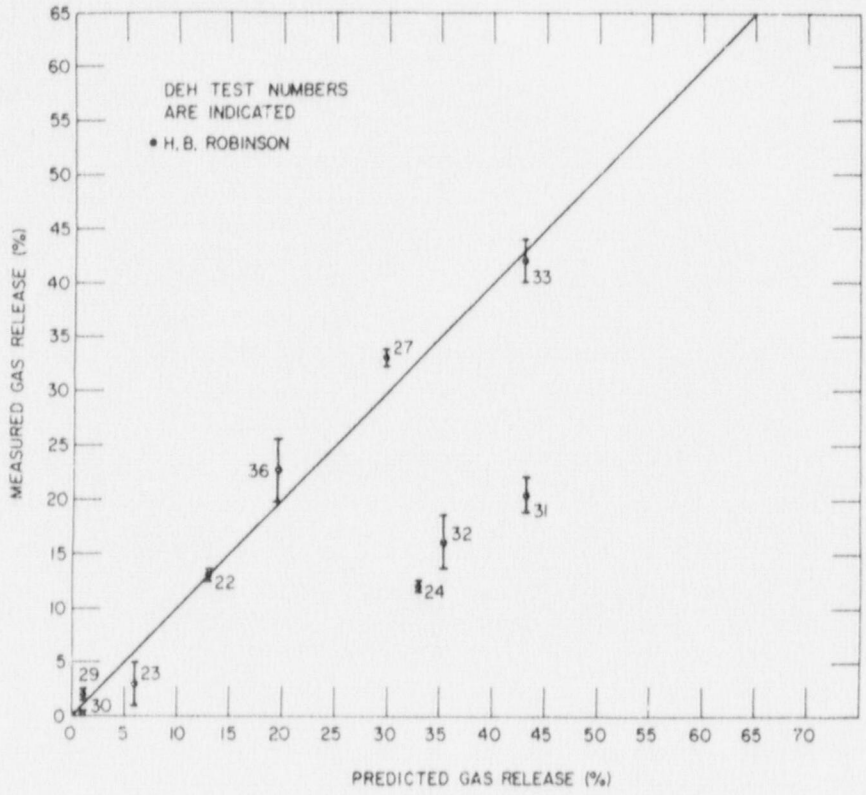

Fig. 20. GRASS-SST-predicted Transient Gas Release Using the Assumed Temperature-dependent Diffusivities Shown in Fig. 19, vs Experimentally Measured Values. These results indicate the need for a dependence of heating rate on gas-bubble diffusivity, e.g., as described by Eq. 83 and discussed in the text. Neg. No. MSD-64916.

Figure 18 shows that GRASS-SST predictions of transient gas release are in good agreement with the data; the deviation in the points from the diagonal line appears to be random. The interpretation of the scatter between predicted and measured results, shown in Fig. 18, requires a clear understanding of the uncertainties in GRASS-SST input quantities, e.g., the temperature profiles in the DEH pellets as a function of transient time. Quantitative information about these uncertainties is required for the calculation of horizontal error bars (i.e., the effect of uncertainties in input quantities on calculated results) for the points in Fig. 18.

For example, to predict DEH transient gas release requires two main calculations:

1. The steady-power irradiation of the DEH-test pellet is simulated. To date, this calculation has been performed by using GRASS-SST coupled both thermally and mechanically to an experimental LWR version[46] (LIFE-LWR) of the LIFE[2,3] fuel-behavior code. GRASS-SST and LIFE-LWR are used to simulate the steady-state irradiation of the entire fuel rod; the initial conditions in a specified pellet are then extracted and saved on a direct-access file. The uncertainties involved in generating the initial conditions in the fuel pellet arise from uncertainties in the LIFE-LWR-predicted steady-power fuel temperatures; LIFE-LWR has only received limited verification.

2. The transient DEH test on the irradiated fuel pellet is simulated using GRASS-SST coupled to the DEHTTD code.[60] The DEHTTD code calculates the radial temperature distribution in the fuel pellet as a function of time. This calculation requires knowledge of the electrical and thermal conductivities of the uncracked irradiated UO_2 as a function of temperature. These conductivities are not well known at elevated temperatures. In addition, extensive grain-boundary separation has been observed in DEH-tested pellets.[5-8] These separations change the thermal conductivity of the UO_2 by as much as a factor of two. A simple semiempirical model has been developed to predict the change in the thermal conductivity as a function of time, given the total increase in the pore-solid surface area during the DEH test (see Eqs. 73 and 74). However, considerable uncertainty remains in the calculated temperatures (the calculated center temperature could be off by 100°C or more), and this uncertainty is certainly reflected, in part, in the scatter observed in Fig. 18.

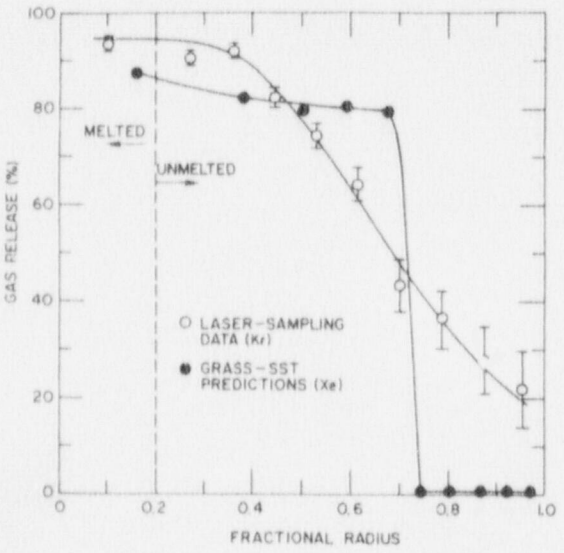

Fig. 21. Radial Profile of Fission-gas Release during DEH Test 33 (from Ref. 66). Neg. No. MSD-65142.

Figure 21 shows GRASS-SST results (xenon) for the radial profile of transient fission-gas release during DEH test 33 plotted with the laser-sampling data (krypton) of Ref. 66. The predicted results show a gradual decrease in fission-gas release from 88% at a fractional radius of 0.16 to 80% at a fractional radius of 0.69. The predicted release then sharply decreases in a step-function-like manner to less than 1% for the rest of the radius. This behavior is in contrast with the relatively smooth decline in the fractional fission-gas release from 82% at a fractional radius of 0.1 to 20% at a fractional radius of 0.90, as shown in Fig. 21. The area under the predicted curve is approximately equal to the area under the experimental curve; this result is reflected in the reasonable GRASS-SST prediction of total transient fission-gas release during test 33 as shown in Fig. 18.

The behavior of the predicted radial profile of transient fission-gas release, as shown in Fig. 21, can be understood in terms of the pore-interlinkage model used in GRASS-SST. This model is based on the assumption that a rapid long-range interconnection of the grain-edge porosity occurs when the gas-bubble fractional swelling exceeds 7% (see Sec. II.F). Thus, the step-function-like decrease in the predicted release at a fractional radius of 0.69 is due to the transition between fuel regions where the gas-bubble swelling was greater than 7% (for fractional radii less than 0.69) to fuel regions where the gas-bubble swelling was less than 7% (for fractional radii greater than 7%).

The qualitative difference between the predicted and experimental results for the radial profile of transient fission-gas release indicates that the GRASS-SST model for the rapid, long-range interconnection of grain-edge porosity is too simple to account for the extensive network of grain-boundary separations observed in DEH-tested fuel. A more realistic calculation of the radial profile of transient fission-gas release would have to include models describing grain-boundary separation as a function of the gas-bubble distribution, the temperature, the fuel microstructure, and the local stresses generated within the fuel pellet.

VIII. HIGH-BURNUP GAS RELEASE

In 1969, Bellamy and Rich[67] presented evidence that, for fuel rods with centerline temperatures less than 1630°C, a large increase in gas release can occur at burnups above 3 at. %. Below 3 at. % burnup, the fission-gas release is compatible with diffusional release and "knockout" models. The marked increase in gas release above 3 at. % was believed to arise in part from the interconnection of grain-boundary gas bubbles and in part from the fracture under thermal stress of grain boundaries weakened by gas bubbles.

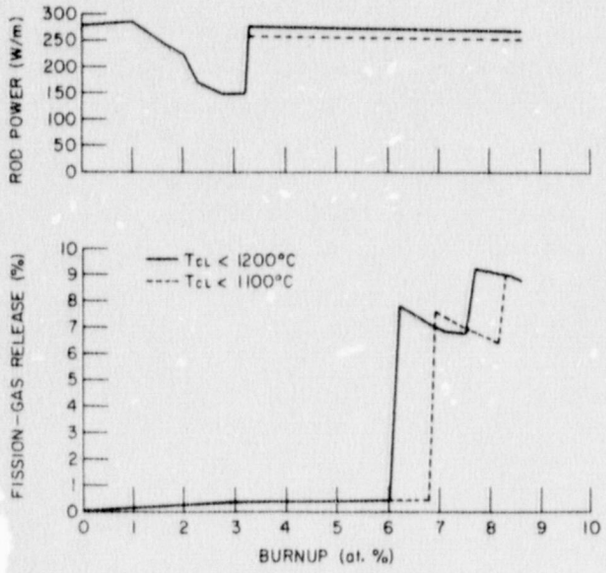

Fig. 22. GRASS-SST Predictions for Gas Release from High-burnup LWR Fuel. Neg. No. MSD-64691.

Phenomena that result in an enhanced rate of fission-gas release during transient heating conditions may also influence steady-state gas release. Figure 22 shows GRASS-SST results for two hypothetical irradiations in the H. B. Robinson reactor (i.e., two extensions of the actual irradiation history). GRASS-SST results for burnups > 5 at. % and centerline temperatures <1200°C indicate that an enhanced release of fission gas occurs from fuel regions in which fission-gas swelling has exceeded an assumed value of ~7% for long-range porosity interconnection (e.g., see Eq. 57). As shown in Fig. 22, the breakaway gas release occurs later for lower-temperature (lower-power) rods. In addition, the breakaway gas release will occur earlier for smaller values of the critical swelling required for long-range porosity interconnection. Other factors, such as the mechanical separation of grain boundaries caused by applied stresses, can influence the amount and the time of breakaway fission-gas release in high-burnup UO_2 fuel.

IX. CONCLUSIONS

GRASS-SST provides a realistic description of fission-gas release and swelling as a function of fuel-fabrication variables and a wide range of operating conditions. GRASS-SST treats fission-gas release and fuel swelling on an equal basis, and simultaneously treats all major mechanisms that influence fission-gas behavior. The GRASS-SST steady-state analysis has undergone verification for end-of-life fission-gas release, fuel swelling, and intragranular bubble-size distributions.

The results of GRASS-SST predictions for transient fission-gas release during DEH tests are in excellent agreement with experimental data. Comparisons of GRASS-SST predictions of gas release and bubble-size distributions with the results of DEH transient tests indicate that (a) coalescing bubbles do not have sufficient time to grow to equilibrium size during most transient conditions, (b) the mobilities of fission-gas bubbles in UO_2 are enhanced during nonequilibrium conditions, if the excess pressure in the bubble is sufficient to generate an equivalent stress greater than or equal to the yield stress of the surrounding matrix, and (c) channel formation on grain surfaces and coalescence of the channels with each other and with the tunnels of gas along the grain edges can contribute to grain-boundary separation and/or the rapid, long-range interconnection of porosity. The phenomenon of grain-boundary separation and/or long-range interconnection of porosity provides an important release mechanism for fission gas that has moved out of the grains of irradiated fuel.

Finally, phenomena that result in an enhanced rate of fission-gas release during transient heating conditions may also influence steady-state gas release at high burnup.

ACKNOWLEDGMENTS

I wish to thank M. C. Billone, S. M. Gehl, C. Y. Li, F. A. Nichols, and R. B. Poeppel for many stimulating discussions. I also wish to thank S. M. Gehl and F. A. Nichols for their critical review of this manuscript.

REFERENCES

1. R. B. Poeppel, "An Advanced Gas Release and Swelling Subroutine," *Proc. Conf. on Fast Reactor Fuel Element Technology*, American Nuclear Society, Hinsdale, IL, pp. 311-326 (1971).

2. V. Z. Jankus and R. W. Weeks, *LIFE-II--A Computer Analysis of Fast-Reactor Fuel-Element Behavior as a Function of Reactor Operating History*, Nucl. Eng. Des. *18*(1), 83-96 (1972).

3. V. Z. Jankus, "Fast-Reactor Fuel-Element Analysis Using Multiregion Formulation in LIFE-II," *2nd Int. Conf. Structural Mechanics in Reactor Technology*, Vol. VI, Part A, Suppl. D2/5, Berlin, Germany (Sept 10-14, 1973).

4. J. Rest, M. G. Seitz, S. M. Gehl, and L. R. Kelman, "Development and Experimental Verification of SST-GRASS: A Steady-State and Transient Fuel Response and Fission-Product Release Code," *Proc. CSNI Specialists Meeting on Behavior of Water Reactor Fuel Elements under Accident Conditions*, Spatind, Norway (Sept 13-16, 1976).

5. S. M. Gehl, M. G. Seitz and J. Rest, "Relationship Between Fission-Gas Release and Microstructural Change During Transient Heating of Pressurized Water Reactor Fuel," *Proc. ANS Topical Meet. Thermal Reactor Safety*, 1977, CONF-770708, Vol. 3, pp. 3-261 to 3-282 (July 31-Aug 5, 1977).

6. J. Rest, M. G. Seitz, and S. M. Gehl, *Release of Fission Gas from High-Burnup Fuel During Transient Heating*, Trans. Am. Nucl. Soc. *26*, 320-324 (1977).

7. S. M. Gehl, M. G. Seitz, and J. Rest, *Fission-gas Release from Irradiated PWR Fuel during Simulated PCM-type Accidents: Progress Report*, NUREG/CR-0088, ANL-77-80 (Apr 1978).

8. J. Rest and S. M. Gehl, "The Mechanistic Prediction of Transient Fission-Gas Release from LWR Fuel," *Proc. IAEA Spec. Meet. Fuel Element Modeling* (Mar 1978); also to be published in J. Nucl. Eng. Design.

9. J. Rest and S. M. Gehl, *Mobility of Fission-Gas Bubbles During Transient Heating Conditions*, Trans. Am. Nucl. Soc. *28*, 239-240 (1978).

10. W. L. Wang, J. Rest, and G. Bandyopadyay, *Transient Fission-Gas Behavior: Experimental and Analytical Results*, Trans. Am. Nucl. Soc. *28*, 240-241 (1978).

11. *The Role of Fission Gas Release in Reactor Licensing*, NUREG-75/077, Core Performance Branch, U. S. Nuclear Regulatory Commission (Nov 1975).

12. A. H. Booth, *A Method of Calculating Fission Gas Diffusion from UO_2 Fuel*, Chalk River Report, CRDC-721 (1957).

13. W. A. Yuill, V. F. Baston, and J. H. McFadden, Idaho Nuclear Report, IN-1467 (1971).

14. J. R. MacEwan and W. H. Stevens, J. Nucl. Mater. *11*, 77 (1964).

15. R. M. Carroll, R. B. Perez, and O. Sisman, J. Am. Ceram. Soc. *48*, 55 (1965).

16. R. S. Barnes and D. J. Mazey, *Electron Microscopy 1964, Vol. A, Proc. Conf., Prague, 1964*, Czech. Acad. Sci., Prague, p. 197 (1964).

17. A. D. Whapham, Nucl. Appl. Technol. *2*, 123 (1966).

18. J. A. Turnbull and M. O. Tucker, *Swelling in UO_2 Under Conditions of Gas Release*, Phil. Mag. *30*, 47 (1972).

19. W. B. Beere and G. L. Reynolds, *The Morphology and Growth Rate of Interlinked Porosity in Irradiated UO_2*, J. Nucl. Mater. *47*, 51 (1973).

20. T. S. Roth and R. B. Poeppel, Argonne National Laboratory, private communication.

21. E. E. Gruber, *Calculated Size Distributions for Gas Bubble Migration and Coalescence in Solids*, J. Appl. Phys. *38*, 243-250 (1967).

2. R. S. Nelson, *The Stability of Gas Bubbles in an Irradiation Environment*, J. Nucl. Mater. *31*, 153-161 (1969).

23. C. C. Dollins and F. A. Nichols, *Swelling and Gas Release in UO_2 at Low and Intermediate Temperatures*, J. Nucl. Mater. *66*, 143-157 (1977).

24. D. R. Olander, *Fundamental Aspects of Nuclear Reactor Fuel Elements*, TID-26711-P1, 214-215 (1976).

25. R. W. Weeks, R. O. Scattergood, and S. R. Pati, *Migration Velocities of Bubble-Defect Configurations in Nuclear Fuels*, J. Nucl. Mater. *38*(2), 223-229 (1970).

26. M. V. Speight, *A Calculation on the Migration of Fission Gas in Material Exhibiting Precipitation and Re-Solution of Gas Atoms Under Irradiation*, Nucl. Sci. Eng. *37*, 180-185 (1969).

27. W. L. Wang and R. N. Singh, *Relaxation Theory of Nonequilibrium Fission Gas Bubbles and Criteria for Equilibrium*, J. Nucl. Mater. (to be published).

28. G. Bandyopadhyay, *Fuel and Fission-Gas Response to Simulated Thermal Transients: Experimental Results and Correlation with Fission-Gas Release and Swelling Model*, J. Nucl. Tech. *44*, 62-78 (1978).

29. M. W. Finnis, M. R. Hayns, and R. Bullough, *The Response of Fission Gas Bubbles to Rapid Heating*, AERE-R-7970 (1975).

30. M. G. Seitz, S. M. Gehl, and C. H. Gebo, "Posttest Microstructure," *Light Water Reactor Safety Research Program: Quarterly Progress Report, April-June 1976*, ANL-76-87, pp. 20-24.

31. J. C. Fisher, *Calculation of Diffusion Penetration Curves for Surface and Grain Boundary Diffusion*, J. Appl. Phys. *22*, 74-77 (1951).

32. K. Maschke, H. Overhof, and P. Thomas, *A Note on Percolation Probabilities*, Phys. Status Solidi (b) *60*, 563 (1973).

33. C. Ronchi, "Definition and Evaluation of the Pore-interlinkage Parameter," *Light-Water-Reactor Safety Research Program: Quarterly Progress Report, July-September 1975*, ANL-75-72, pp. 94-96.

34. J. A. Turnbull, *A Review of Rare Gas Diffusion in Uranium Dioxide*, RD/B/N2406 (1972).

35. M. E. Gulden, *Migration of Gas Bubbles in Irradiated Uranium Dioxide*, J. Nucl. Mater. *23*, 30-36 (1967).

36. L. E. Willertz and P. G. Shewmon, *Diffusion of Helium Gas Bubbles in Gold and Copper Foils*, Met. Trans. *1*, 2217-2223 (1970).

37. W. Oldfield and J. B. Brown, Jr., *Bubble Migration in UO_2--A Study Using a Laser Image Furnace*, Mater. Sci. Eng. *6*, 361-370 (1970).

38. W. Beere, *Transport Kinetics in Faceted Bubbles*, J. Nucl. Mater. *45*, 91-95 (1973).

39. W. Beere and G. L. Reynolds, *Rate Controlling Nucleation and Diffusion Processes in Faceted Inert Gas Bubbles and Voids*, Acta Metall. *20*, 845-858 (1972).

40. R. M. Cornell, *The Growth of Fission Gas Bubbles in Irradiated Uranium Dioxide*, Phil. Mag. *19*, 539 (1969).

41. A. Hölt and H. J. Matzke, *Fission-Enhanced Self-Diffusion of Uranium in UO_2 and UC*, J. Nucl. Mater. *48*, 157 (1973).

42. R. M. Cornell, *An Electron Microscope Examination of Matrix Fission-Gas Bubbles in Irradiated Uranium Dioxide*, J. Nucl. Mater. *38*, 319 (1971).

43. J. Rest, *Behavior of Fission Gas in LWR Fuel During Steady-State Operating Conditions*, Trans. Am. Nucl. Soc. *23*(1), 171-172 (June 1976).

44. J. W. Harrison, *An Extrapolated Equation of State for Xenon for Use in Fuel Swelling Calculations*, J. Nucl. Mater. *31*, 99-106 (1969).

45. E. M. Baroody, *Calculations on the Collisional Coalescence of Gas Bubbles in Solids*, J. Appl. Phys. *38*, 4893-4903 (1967).

46. J. Rest, *SST: A Computer Code to Predict Fuel Response and Fission Product Release from Light-Water Reactor Fuels During Steady-State and Transient Conditions*, Trans. Am. Nucl. Soc. *22*(1), 462-463 (Nov 1975).

47. S. M. Gehl, *ANL-EG&G Crosscheck of Nuclear and Electrical Heating*, to be published as ANL-78-60 (1978).

48. P. Nikolopoulos, S. Nazare, and F. Thümmler, *Surface, Grain Boundary and Interfacial Energies in UO_2 and UO_2-Ni*, J. Nucl. Mater. *71*, 89-94 (1977).

49. C. Ronchi and H. J. Matzke, "Calculations and Estimates of Contributions of Different Transport Mechanisms to Fission-Gas Behavior in Fast Breeder Oxide Fuel," *Fuel and Fuel Elements for Fast Reactors*, Vol. 1, IAEA, Vienna, p. 57 (1974).

50. J. A. Turnbull, *The Effect of Grain Size on the Swelling and Gas Release Properties of UO_2 During Irradiation*, J. Nucl. Mater. *50*, 62-68 (1974).

51. M. V. Speight, *A Calculation of the Size Distribution of Intragranular Bubbles in Irradiated UO_2*, J. Nucl. Mater. *38*, 236-238 (1971).

52. C. Ronchi and H. J. Matzke, *Calculation of the In-Pile Behavior of Fission Gas in Oxide Fuels*, J. Nucl. Mater. *45*, 15-28 (1973).

53 J. A. Turnbull and R. M. Cornell, *Observations Demonstrating the Re-Solution of Gas from Bubbles and Sintering Pores During the Irradiation of UO_2 at a High Temperature*, J. Nucl. Mater. *37*, 355-357 (1970).

54. S. R. Pati, M. J. Dapht, and D. R. O'Boyle, *Re-Solution-Controlled Fission Gas Behavior in UO_2 Irradiated in a Fast Flux*, J. Nucl. Mater. *50*, 227-246 (1974).

55. S. M. Gehl, R. N. Blomquist, M. G. Seitz, and D. S. Butler, "Fission-product Characterization," *Light-Water-Reactor Safety Research Program: Quarterly Progress Report, July-September 1975*, ANL-72, pp. 42-44.

56. R. A. Lorenz, J. L. Collins, and S. R. Manning, *Quarterly Progress Report on Fission Product Release from LWR Fuel for the Period October-December 1975*, ORNL/TM-5290 (Mar 1976).

57. G. W. Gibson et al., ANCR-NUREG-1321 (1976).

58. D. Freund and W. Schikarski, KFK01031, EURFNR-773 (1970).

59. B. J. Wrona and E. Johanson, Nucl. Technol. *29*, 433 (1976).

60. J. C. Voglewede, Argonne National Laboratory, private communication.

61. A. B. G. Washington, *Preferred Values for Thermal Conductivity of Sintered Ceramic Fuel for Fast Reactor Use*, UKAEA TRG-Report-2236 (Sept 1973).

62. S. M. Gehl, Argonne National Laboratory, private communication.

63. C. Baker, J. Nucl. Mater. *71*, 117-123 (1977).

64. W. G. Beere, *The Nucleation of Atomic Steps on Inert Gas Bubbles Intersected by Dislocations*, Phil. Mag. *25*, 189-200 (1972).

65. J. T. A. Roberts, "High-Temperature Plasticity of Oxide Nuclear Fuel," *Symposium on Plastic Deformation of Ceramics*, The Pennsylvania State University (1974).

66. S. M. Gehl and D. G. Graczyk, "Determination of Radial Fission-gas Profiles for DEH-tested Fuel," *Light-Water-Reactor Safety Research Program: Quarterly Progress Report, October-December 1977*, ANL-78-25, pp. 16-19 (May 1978).

67. R. G. Bellamy and J. B. Rich, *Grain-Boundary Gas Release and Swelling in High Burnup Uranium Dioxide*, J. Nucl. Mater. *33*, 64-76 (1969).